Data on unveiling the occurrence of transient, multi-contaminated mafic magmas inside a rhyolitic reservoir feeding an explosive

Data in Brief xxx (xxxx) xxx

Contents lists available at ScienceDirect

Data in Brief

journal homepage: www.elsevier.com/locate/dib

Data Article

Data on unveiling the occurrence of transient, multi-contaminated mafic magmas inside a rhyolitic reservoir feeding an explosive eruption (Nisyros, Greece)

Q1 Q2 F. Mastroianni[a,b,*], E. Braschi[c,**], M. Casalini[b], S. Agostini[d], S. Di Salvo[b], G. Vougioukalakis[e], L. Francalanci[b]

Q3 [a] *Dipartimento di Scienze della Terra, Università di Pisa, Via S. Maria, 53, Pisa 56126, Italy*
[b] *Dipartimento di Scienze della Terra, Università degli studi di Firenze, Via Giorgio La Pira, 4, Firenze 50121, Italy*
[c] *Istituto di Geoscienze e Georisorse, Consiglio Nazionale delle Ricerche, sede secondaria di Firenze, Via Giorgio La Pira, 4 50121, Italy*
[d] *Istituto di Geoscienze e Georisorse, Consiglio Nazionale delle Ricerche, sede di Pisa, Via G. Moruzzi, 1 56124, Italy*
[e] *Hellenic Survey of Geology and Mineral Exploration, 3rd Entrance Olympic village 13637, Aharne, Athens, Greece*

ARTICLE INFO

Article history:
Received 8 February 2022
Revised 16 March 2022
Accepted 17 March 2022
Available online xxx

Dataset link: Data on the juvenile products of the Upper Pumice eruption on Nisyros (Braschi et al., 2022) (Original data)

ABSTRACT

This data article includes the description and the geochemical and mineralogical dataset of 67 pyroclastic rock samples from the Upper Pumice (UP) explosive activity of Nisyros volcano (eastern South Aegean Active Volcanic Arc). A detailed field and petrographic description of the studied outcrops and samples are reported, including representative photomicrographs and SEM images, whole-rock major and trace elements compositions of 31 representative samples and Sr-Nd isotope ratios on 22 selected samples. Analytical methods and conditions used for data acquisition are also reported.
The UP eruption produced a stratigraphic sequence constituted by a basal fallout deposit, gradually substituted by pyroclastic density current (PDC) deposits; these are overlaid by a lag-breccia unit, and the sequence is closed by a grey ash flow level. The juvenile is mainly constituted by

DOI of original article: 10.1016/j.lithos.2021.106574
* Corresponding author at: Dipartimento di Scienze della Terra, Università di Pisa, Via S. Maria, 53, Pisa 56126, Italy.
** Corresponding author.
E-mail addresses: filippo.mastroianni@phd.unipi.it (F. Mastroianni), eleonora.braschi@igg.cnr.it (E. Braschi).

https://doi.org/10.1016/j.dib.2022.108077

Please cite this article as: F. Mastroianni, E. Braschi and M. Casalini et al., Data on unveiling the occurrence of transient, multi-contaminated mafic magmas inside a rhyolitic reservoir feeding an explosive eruption (Nisyros, Greece), Data in Brief, https://doi.org/10.1016/j.dib.2022.108077

white-yellow, moderately crystalline pumice with rhyolitic composition and homogenous Sr-Nd isotope values. Variable amounts of dense, grey, crystalline juvenile lapilli clasts (CRC, Crystal-Rich Clast), with rounded shape and less evolved composition (andesite to dacite) are also present in the deposit. These mafic CRCs are peculiar due to their large variability in textures (from distinctive diktytaxitic to strongly fragmented structure without a defined fabric) and in the geochemical and isotopic composition.

The data acquired were fundamental to reconstruct the complex and peculiar history of ascent, storage and differentiation/assimilation processes of these mafic melts before their intrusion into the shallow, rhyolitic magma chamber, with important implication on the possible eruption trigger during the more recent explosive phase of activity at Nisyros volcano. Moreover, the geochemical and isotopic analyses provide new original data to the general knowledge of the Aegean volcanics.

All the data reported in this paper are related to the research article Braschi et al.

Specifications Table

Subject area	Earth and Planetary Sciences
Specific subject area	Geochemistry and Petrology
Type of data	Text files, pictures, tables and graphs.
How data was acquired	Field work: detailed sampling and deposit description during two field campaigns. Petrographic analyses through polarized light microscopy. Image acquisition through scanning electron microscope (SEM). Laboratory measurements: Sr isotope composition through Thermal Ionization Mass Spectrometry (TIMS) and Nd isotope composition through Multicollector Inductively Coupled Plasma Mass Spectrometry (MC-ICP-MS). Major and minor composition of mineral phases through Electron Microprobe Analysis (EPMA).
Data format	Raw and analysed
Description of data collection	All data are originals and were collected by the authors using accepted procedures and robust analytical condition. Details of data collection are reported in the “Experimental Design, Materials, and Methods” section.
Data source location	Institution: Istituto di Geoscienze e Georisorse, Sezione di Firenze; Dipartimento di Scienze della Terra, Università degli Studi di Firenze. City/Town/Region: Firenze Country: Italy Latitude and longitude (and GPS coordinates, if possible) for collected samples/data: 36.58905° N, 27.16918° E Nisyros Island, Dodecanese, Greece
Data accessibility	Repository name: EarthChem Library Data identification number (permanent identifier, i.e. DOI number): DOI: 10.26022/IEDA/112,230. Direct link to the dataset: https://ecl.earthchem.org/view.php?id=2230.
Related research article	E. Braschi, F. Mastroianni, S. Di Salvo, M. Casalini, S. Agostini, G. E. Vougioukalakis, L. Francalanci, Unveiling the occurrence of transient, multi-contaminated mafic magmas inside a rhyolitic reservoir feeding an explosive eruption (Nisyros, Greece), Lithos 410–411 (2022) 106,574. https://doi.org/10.1016/j.lithos.2021.106574

Please cite this article as: F. Mastroianni, E. Braschi and M. Casalini et al., Data on unveiling the occurrence of transient, multi-contaminated mafic magmas inside a rhyolitic reservoir feeding an explosive eruption (Nisyros, Greece), Data in Brief, https://doi.org/10.1016/j.dib.2022.108077

Value of the Data

- These data are crucial for the reconstruction of the plumbing system dynamic of Nisyros Volcano before the Upper Pumice eruption.
- The data, including mineral chemistry and Sr-Nd isotope ratios, expand and integrate the existent database of volcanic products of the South Aegean Active Volcanic Arc.
- Crystal-rich clasts (CRC) show the lowest 143Nd/144Nd values recorded for the Nisyros-Kos-Yali volcanic field.
- The data will contribute to a better understanding of the involvement of different crustal components and ascent pathways of mafic magmas below active volcanoes in subduction zones.

1. Data and Images

Data, images and figures here reported were interpreted and discussed in Braschi et al. [1] to unravel the origin and evolution of the mafic components erupted by the UP activity, and their interaction with the main rhyolitic host magma. The full dataset of major, trace elements and Sr-Nd isotopes on whole rocks, together with glass composition and mineral chemistry is available in the EarthChem Library repository at https://doi.org/10.26022/IEDA/112230.

1.1. Field observation

Table 1 is a list of the samples collected from the Upper Pumice (UP) deposit. The table reports detailed information of the sampling locations for the different outcrops (see also Fig. 1), including the type of depositional unit. A schematic petrographic description of each sample is also reported including their structure, paragenesis and texture features. Some samples have been subdivided into different portions according to their characteristics and labelled with different letters.

Representative photos of the sampled outcrops of the UP deposit are shown in Figs. 2–8 and illustrate in detail the different depositional units emplaced by the UP eruption and their juvenile components.

Figs. 9–12 report selected representative images of cut blocks of samples and hand-specimen highlighting the difference between the two main lithotypes (pumice and crystal-rich clasts, hereafter CRCs) and within the CRC population itself. The CRCs show wide variation in their vesiculation and colour; the latter is due to the different proportion of crystal content (both for phases and size) and groundmass, varying from grey to white.

1.2. Petrography

In the next section, a detailed selection of microphotographs and backscattered (BSE) images (Figs. 13–22) are reported to show the main petrographic characteristics of the studied samples (pumices and CRCs).

Pumices from all the deposits have similar features. They are porphyritic, mainly composed by a glassy matrix and a crystal content up to 5–10%; vesicularity vary between 30% and 50%; the matrix appears often fibrous or fluidal. Paragenesis is mainly composed by plagioclase (always more than 75%), orthopyroxene and amphibole; clinopyroxene and olivine are rare; accessory phases are oxides and apatite, often included in orthopyroxene. Crystals are often found as glomeroporphyritic aggregates. Plagioclase phenocrysts sometimes show disequilibrium textures, with sieved cores, resorbed zones, resorbed or overgrowth rims.

Please cite this article as: F. Mastroianni, E. Braschi and M. Casalini et al., Data on unveiling the occurrence of transient, multi-contaminated mafic magmas inside a rhyolitic reservoir feeding an explosive eruption (Nisyros, Greece), Data in Brief, https://doi.org/10.1016/j.dib.2022.108077

Table 1
Location and petrographic description of the studied samples from the Upper Pumice deposit (Nisyros, Greece). *Footnotes*: * samples with mingling evidences are doubled to describe crystal-rich and pumiceous portions: "-" thin section not available. CRC: Crystal-rich clast; Plg: plagioclase; Cpx: clinopyroxene; Opx: orthopyroxene; Amph: amphibole; Ol: olivine; Ox: oxides; ph: phenocrysts (crystals >0.5 mm); mph: micro-phenocrysts (crystals >0.3 mm). Reaction rims: presence of olivines and/or opx with reaction rims to amphiboles; ph+mph in CRC (%): estimated abundance of crystals coarser than the average size of the microcrystalline groundmass in the CRCs.

Sample	Sampling location	Coordinates	Elevation m s.l.m.	Outcrop	Depositional Unit	Lithology	Sample size	Sample Texture	CRC Texture Type	Paragenesis	plg/femic	Cristallinity (vol. %)	Vacuolarity (vol. %)	Glass (vol. %)	Crystal Aggregates	(Micro-) Enclaves	Reaction rim	ph+mph in CRC (vol. %)	
NIS312	Cape Katzouni	36°36′55.38″N	27°11′25.52″E	18	8	Lag-breccia	Crystal rich clast	ca. 20 cm		Type-C	Plg, Cpx, Ox, Ol, Opx, Amph	65/35	45	45	10	✓		✓	1
NIS313	Cape Katzouni	36°36′55.38″N	27°11′25.52″E	18	8	Lag-breccia	Crystal rich clast			Type-C	Plg, Cpx, Ox, Opx, Amph	35/35	45	40	15	✓			5
NIS314	Cape Katzouni	36°36′55.38″N	27°11′25.52″E	18	8	Lag-breccia	Crystal rich clast			Type-B	Plg, Cpx, Ox, Ol, Amph	55/45	37	53	10	✓		✓	10
NIS315	Pali - main road	36°37′0.10″N	27° 9′57.52″E	38	5	Fallout	Pumice		porphyritic		Plg, Opx, Cpx, Amph, Ox	90/10	5	50	45				
NIS316a	Pali - main road	36°37′0.10″N	27° 9′57.52″E	38	5	Fallout	Crystal rich clast			Type-A	Plg, Cpx, Ox, Ol, Opx, Amph	60/40	40	50	10		✓		20
NIS316b	Pali - main road	36°37′0.10″N	27° 9′57.52″E	38	5	Fallout	Crystal rich clast			Type-B	Plg, Cpx, Ox, Opx, Amph	60/40	45	45	10		✓		15
NIS316c	Pali - main road	36°37′0.10″N	27° 9′57.52″E	38	5	Fallout	Crystal rich clast			Type-B	Plg, Cpx, Ox, Opx, Amph	90/10	40	45	15		✓		7
NIS316d	Pali - main road	36°37′0.10″N	27° 9′57.52″E	38	5	Fallout	Crystal rich clast			Type-B	Plg, Cpx, Ox, Opx, Amph	85/15	38	52	10		✓	✓	1
NIS316e	Pali - main road	36°37′0.10″N	27° 9′57.52″E	38	5	Fallout	Crystal rich clast			Type-B	Plg, Cpx, Ox, Opx, Amph	95/5	15	65	20				1
NIS316f	Pali - main road	36°37′0.10″N	27° 9′57.52″E	38	5	Fallout	Crystal rich clast			Type-A	Plg, Cpx, Ox, Opx, Amph	80/20	30	60	10				
NIS316g	Pali - main road	36°37′0.10″N	27° 9′57.52″E	38	5	Fallout	Crystal rich clast			Type-A	Plg, Cpx, Ox, Opx, Amph	70/30	30	50	20				1
NIS316h	Pali - main road	36°37′0.10″N	27° 9′57.52″E	38	5	Fallout	Crystal rich clast			Type-B	Plg, Cpx, Ox, Opx, Amph	90/10	30	55	15		✓		5
NIS 317	Emborion cemetery	36°36′20.06″N	27°10′21.90″E	362	1	Fallout	Crystal rich clast			Type-A	Plg, Cpx, Ox, Opx, Amph	90/10	30	50	20				
NIS 318	Emborion cemetery	36°36′20.06″N	27°10′21.90″E	362	1	Fallout	Crystal rich clast			Type-B	Plg, Cpx, Ox, Opx, Amph	70/30	25	55	20				1

(*continued on next page*)

Table 1 (*continued*)

Sample	Sampling location	Coordinates	Elevation m s.l.m.	Outcrop	Depositional Unit	Lithology	Sample size	Sample Texture	CRC Texture Type	Paragenesis	plg/femic	Cristallinity (vol. %)	Vacuolarity (vol. %)	Glass (vol. %)	Crystal Aggregates	(Micro-) Enclaves	Reaction rim	ph+mph in CRC (vol. %)	
NIS 353	Emborion cemetery	36°36′20.06″N	27°10′21.90″E	362	1	Fallout	Pumice	5–10 cm	porphyritic		Plg, Opx, Ox, Amph	75/25	15	30	55	√	√		
NIS 354	Emborion cemetery	36°36′20.06″N	27°10′21.90″E	362	1	Fallout	Pumice												
NIS 355	Emborion cemetery	36°36′20.06″N	27°10′21.90″E	362	1	Fallout	Crystal rich clast	ca. 20 cm	vesicular, aphyric	Type-A	Plg, Cpx, Ox, Ol, Opx, Amph	60/40	45	40	15	√		√	10
NIS 356	Emborion cemetery	36°36′20.06″N	27°10′21.90″E	362	1	Fallout	Crystal rich clast	ca. 15 cm	high vesicular, aphyric/microcrystalline	Type-A	Plg, Opx, Cpx, Amph, Ox	65/26	35	50	15	√			30
NIS 357	Emborion cemetery	36°36′20.06″N	27°10′21.90″E	362	1	Fallout	Crystal rich clast	ca. 25 cm	low vesicular, aphyric	Type-B	Plg, Opx, Cpx, Amph, Ox	75/25	55	25	20	√		√	10
NIS 358	Emborion cemetery	36°36′20.06″N	27°10′21.90″E	362	1	Fallout	Crystal rich clast	ca. 15 cm	vesicular, aphyric/microcrystalline	Type-A	Plg, Opx, Cpx, Amph, Ox	70/30	40	45	15			√	1
NIS 358*	Emborion cemetery	36°36′20.06″N	27°10′21.90″E	362	1	Fallout	Pumice	ca. 15 cm	porphyritic		Plg, Opx, Cpx, Amph, Ox	80/20	10	50	40		√		
NIS 359	Emborion cemetery	36°36′20.06″N	27°10′21.90″E	362	1	Fallout	Crystal rich clast	30–40 cm	low vesicular, aphyric	Type-A	Plg, Opx, Cpx, Amph, Ox	70/30	38	45	17	√		√	5
NIS 360	Emborion cemetery	36°36′20.06″N	27°10′21.90″E	362	1	Fallout	Crystal rich clast	5–8 cm	vesicular, microcrystalline	Type-B	Plg, Opx, Cpx, Amph, Ox	80/20	45	37	18	√			5
NIS 361	Emborion cemetery	36°36′20.06″N	27°10′21.90″E	362	1	Fallout	Crystal rich clast	ca. 30 cm	low vesicular, aphyric	Type-A	Plg, Cpx, Ox, Ol, Opx, Amph	50/50	40	45	15				5
NIS 362	Emborion cemetery	36°36′20.06″N	27°10′21.90″E	362	1	Fallout	Crystal rich clast			Type-B	Plg, Cpx, Ox, Ol, Opx, Amph	60/40	40	50	10		√	√	1
NIS 363	Emborion cemetery	36°36′20.06″N	27°10′21.90″E	362	1	Fallout	Crystal rich clast			Type-B	Plg, Cpx, Ox, Ol, Opx, Amph	60/40	25	70	5		√	√	5
NIS 364	Emborion cemetery	36°36′20.06″N	27°10′21.90″E	362	1	Fallout	Crystal rich clast			Type-B	Plg, Cpx, Ox, Ol, Opx, Amph	70/30	30	50	20		√	√	5
NIS 365	Emborion cemetery	36°36′20.06″N	27°10′21.90″E	362	1	Fallout	Crystal rich clast			Type-B	Plg, Cpx, Ox, Ol, Opx, Amph	80/20	40	40	20		√		7
NIS 366	Emborion cemetery	36°36′20.06″N	27°10′21.90″E	362	1	Fallout	Crystal rich clast			-	-	-	-	-	-	-	-	-	-
NIS 367	Emborion cemetery	36°36′20.06″N	27°10′21.90″E	362	1	Fallout	Crystal rich clast			-	-	-	-	-	-	-	-	-	-

(*continued on next page*)

Please cite this article as: F. Mastroianni, E. Braschi and M. Casalini et al., Data on unveiling the occurrence of transient, multi-contaminated mafic magmas inside a rhyolitic reservoir feeding an explosive eruption (Nisyros, Greece), Data in Brief, https://doi.org/10.1016/j.dib.2022.108077

JID: DIB ARTICLE IN PRESS [mUS1Ga;March 28, 2022;14:33]

Table 1 (*continued*)

Sample	Sampling location	Coordinates	Elevation m s.l.m.	Outcrop	Depositional Unit	Lithology	Sample size	Sample Texture	CRC Texture Type	Paragenesis	plg/femic	Cristallinity (vol. %)	Vacuolarity (vol. %)	Glass (vol. %)	Crystal Aggregates	(Micro-) Enclaves	Reaction rim	ph+mph in CRC (vol. %)	
NIS 368	Emborion cemetery	36°36′20.06″N	27°10′21.90″E	362	1	Fallout	Crystal rich clast			Type-B	Plg, Cpx, Ox, Ol, Opx, Amph	75/25	40	45	15				10
NIS 370	Main road	36°36′38.78″N	27°10′39.86″E	151	2	Fallout	Crystal rich clast	30–40 cm	vesicular, aphyric/microcrystalline	Type-A	Plg, Opx, Amph, Ox	70/30	30	60	10				10
NIS 371	Main road	36°36′38.78″N	27°10′39.86″E	151	2	Fallout	Crystal rich clast	ca. 30 cm	vesicular, aphyric	Type-A	Plg, Opx, Cpx, Amph, Ox	70/30	32	56	12	✓			10
NIS 372b	Main road	36°36′38.78″N	27°10′39.86″E	151	2	Fallout	Crystal rich clast		low vesicular, aphyric/microcrystalline	Type-C	Plg, Cpx, Ox, Ol, Opx, Amph	60/40	45	45	10		✓	✓	3
NIS 374	Lateral valley	36°36′40.55″N	27°10′34.57″E	159	3	Fallout	Pumice		porphyritic		Plg, Opx, Cpx, Amph, Ox	93/7	7	40	53	✓	✓		
NIS 375	Lateral valley	36°36′40.55″N	27°10′34.57″E	159	3	Fallout	Crystal rich clast		high vesicular, aphyric/microcrystalline	Type-A	Plg, Opx, Cpx, Amph, Ox	70/30	30	60	10				5
NIS 377	Caldera rim	36°36′16.64″N	27° 9′56.06″E	323	4	Fallout	Pumice	6–30 cm	porphyritic		Plg, Opx, Cpx, Amph, Ox	80/20	10	35	55	✓	✓		
NIS 378	Caldera rim	36°36′16.64″N	27° 9′56.06″E	323	4	Fallout	Crystal rich clast	ca. 40 cm	vesicular, aphyric/microcrystalline	Type-A	Plg, Cpx, Ox, Ol, Amph	60/40	50	30	20	✓			10
NIS 378*	Caldera rim	36°36′16.64″N	27° 9′56.06″E	323	4	Fallout	Pumice	ca. 40 cm	porphyritic		Plg, Opx, Amph, Ox	90/10	5	45	50	✓	✓		
NIS 379b	Caldera rim	36°36′16.64″N	27° 9′56.06″E	323	4	Fallout	Crystal rich clast	ca. 10 cm	low vesicular, microcrystalline	Type-C									
NIS 380	Caldera rim	36°36′16.64″N	27° 9′56.06″E	323	4	Fallout	Crystal rich clast	ca. 30 cm	low vesicular, aphyric/microcrystalline	Type-A	Plg, Opx, Cpx, Amph, Ox	65/35	25	60	15		✓		
NIS 381	Caldera rim	36°36′16.64″N	27° 9′56.06″E	323	4	Fallout	Crystal rich clast	ca. 40 cm	low vesicular, aphyric	Type-A	Plg, Cpx, Ox, Ol, Opx, Amph	75/25	38	42	20				15
NIS 381*	Caldera rim	36°36′16.64″N	27° 9′56.06″E	323	4	Fallout	Pumice	ca. 40 cm	porphyritic		Plg, Cpx, Ox, Ol, Opx, Amph	85/15	10	40	50	✓	✓		
NIS 383	Caldera rim	36°36′16.64″N	27° 9′56.06″E	323	4	Fallout	Pumice		porphyritic, banded	Type-A	Plg, Cpx, Ox, Ol, Opx, Amph	65/35	40	45	15				10
NIS 385	Caldera rim	36°36′16.64″N	27° 9′56.06″E	323	4	Fallout	Crystal rich clast		low vesicular, aphyric/microcrystalline	Type-A	Plg, Opx, Cpx, Amph, Ox	70/30	40	45	15				2
NIS 390	Caldera rim	36°36′16.64″N	27° 9′56.06″E	323	4	Fallout	Pumice		banded										
NIS 401	Loutra - Gas station	36°36′43.67″N	27° 9′24.27″E	35	6	Fallout	Pumice		porphyritic		Plg, Cpx, Ox, Ol, Opx, Amph	96/4	10	40	50	✓	✓		

(*continued on next page*)

Please cite this article as: F. Mastroianni, E. Braschi and M. Casalini et al., Data on unveiling the occurrence of transient, multi-contaminated mafic magmas inside a rhyolitic reservoir feeding an explosive eruption (Nisyros, Greece), Data in Brief, https://doi.org/10.1016/j.dib.2022.108077

Table 1 (*continued*)

Sample	Sampling location	Coordinates	Elevation m s.l.m.	Outcrop	Depositional Unit	Lithology	Sample size	Sample Texture	CRC Texture Type	Paragenesis	plg/femic	Cristallinity (vol. %)	Vacuolarity (vol. %)	Glass (vol. %)	Crystal Aggregates	(Micro-) Enclaves	Reaction rim	ph+mph in CRC (vol. %)	
NIS 402	Loutra - Gas station	36°36′43.67″N	27° 9′24.27″E	35	6	Fallout	Pumice												
NIS 409	Road to Cape Katzouni	36°37′2.19″N	27°11′17.11″E	34	7a	Lag-breccia	Pumice												
NIS 413	Road to Cape Katzouni	36°37′2.19″N	27°11′17.11″E	34	7a	Lag-breccia	Crystal rich clast	2–3 cm		Type-C	Plg, Cpx, Ox, Ol, Opx, Amph	80/20	45	45	10				2
NIS 416	Road to Cape Katzouni	36°37′2.19″N	27°11′17.11″E	34	7a	Lag-breccia	Crystal rich clast	>20 cm	vesicular, microcrystalline	Type-C	Plg, Cpx, Ox, Opx, Amph	70/30	35	55	10	✓			10
NIS 418	Cape Katzouni	36°36′55.38″N	27°11′25.52″E	18	8	Lag-breccia	Pumice	ca. 50 cm	porphyritic		Plg, Cpx, Ox, Opx, Amph	93/7	5	52	43			✓	
NIS 419	Cape Katzouni	36°36′55.38″N	27°11′25.52″E	18	8	Lag-breccia	Pumice	ca. 10 cm	porphyritic		Plg, Cpx, Ox, Ol, Opx, Amph	93/7	10	50	40	✓	✓		
NIS 420b	Cape Katzouni	36°36′55.38″N	27°11′25.52″E	18	8	Lag-breccia	Crystal rich clast	4–10 cm	vesicular, aphyric/microcrystalline	Type-A	Plg, Cpx, Ox, Opx, Amph	85/15	45	40	15				5
NIS 421	Cape Katzouni	36°36′55.38″N	27°11′25.52″E	18	8	Lag-breccia	Crystal rich clast	>40 cm	low vesicular, microcrystalline	Type-C	Plg, Cpx, Ox, Opx, Amph	70/30	50	40	10	✓		✓	15
NIS 422	Cape Katzouni	36°36′55.38″N	27°11′25.52″E	18	8	Lag-breccia	Crystal rich clast	>40 cm	low vesicular, microcrystalline	Type-C	Plg, Cpx, Ox, Opx, Amph	65/35	50	40	10	✓		✓	
NIS 423	Cape Katzouni	36°36′55.38″N	27°11′25.52″E	18	8	Lag-breccia	Crystal rich clast	ca. 15 cm	vesicular, microcrystalline	Type-B	Plg, Cpx, Ox, Ol, Opx, Amph	80/20	35	55	10	✓			15
NIS 424	Cape Katzouni	36°36′55.38″N	27°11′25.52″E	18	8	Lag-breccia	Crystal rich clast	ca. 40 cm	vesicular, microcrystalline	Type-B	Plg, Cpx, Ox, Ol, Opx, Amph	65/35	40	45	15	✓		✓	5
NIS 425	Cape Katzouni	36°36′55.38″N	27°11′25.52″E	18	8	Lag-breccia	Crystal rich clast		vesicular, aphyric/microcrystalline	Type-C	Plg, Cpx, Ox, Ol, Opx, Amph		50	40	10				
NIS 426	Cape Katzouni	36°36′55.38″N	27°11′25.52″E	18	8	Lag-breccia	Crystal rich clast	ca. 15 cm	vesicular, microcrystalline	Type-C	Plg, Cpx, Ox, Ol, Opx, Amph	55/45	45	40	15	✓		✓	10

(*continued on next page*)

Please cite this article as: F. Mastroianni, E. Braschi and M. Casalini et al., Data on unveiling the occurrence of transient, multi-contaminated mafic magmas inside a rhyolitic reservoir feeding an explosive eruption (Nisyros, Greece), Data in Brief, https://doi.org/10.1016/j.dib.2022.108077

Table 1 (*continued*)

Sample	Sampling location	Coordinates	Elevation m s.l.m.	Outcrop	Depositional Unit	Lithology	Sample size	Sample Texture	CRC Texture Type	Paragenesis	plg/femic	Cristallinity (vol. %)	Vacuolarity (vol. %)	Glass (vol. %)	Crystal Aggregates	(Micro-) Enclaves	Reaction rim	ph+mph in CRC (vol. %)	
NIS 427	Cape Katzouni	36°36′55.38″N	27°11′25.52″E	18	8	Lag-breccia	Crystal rich clast	ca. 40 cm	vesicular, microcrystalline	Type-C	Plg, Cpx, Ox, Ol, Opx, Amph	75/25	43	45	12	✓		✓	5
NIS 428	Cape Katzouni	36°36′55.38″N	27°11′25.52″E	18	8	Lag-breccia	Crystal rich clast	ca. 15 cm	high vesicular, microcrystalline	Type-C	Plg, Cpx, Ox, Ol, Opx, Amph	50/50	40	45	15				5
NIS 429	Cape Katzouni	36°36′55.38″N	27°11′25.52″E	18	8	Lag-breccia	Crystal rich clast	10–15 cm	low vesicular, aphyric	Type-B	Plg, Ox, Opx, Amph	60/40	45	35	20			✓	15
NIS 430	Cape Katzouni	36°36′55.38″N	27°11′25.52″E	18	8	Lag-breccia	Crystal rich clast	ca. 10 cm	low vesicular, aphyric/microcrystalline	Type-B	Plg, Cpx, Ox, Ol, Amph	60/40	45	40	15			✓	10
NIS 431	Nikia - main road	36°34′47.52″N	27°11′16.38″E	421	9	Diluted PDC	Pumice	ca. 20 cm	porphyritic		Plg, Cpx, Ox, Opx, Amph	95/5	7	45	48	✓	✓		
NIS 433	Nikia - main road	36°34′47.52″N	27°11′16.38″E	421	9	Diluted PDC	Pumice	ca. 40 cm	porphyritic		Plg, Cpx, Ox, Opx, Amph	95/5	5	50	45	✓	✓		
NIS 434	Nikia - main road	36°34′47.52″N	27°11′16.38″E	421	9	Diluted PDC	Crystal rich clast		vesicular, aphyric/microcrystalline	Type-B	Plg, Cpx, Ox, Ol, Opx, Amph	85/15	35	55	10		✓	✓	2
NIS 435	Nikia - main road	36°34′47.52″N	27°11′16.38″E	421	9	Diluted PDC	Crystal rich clast	6–8 cm	low vesicular, aphyric/microcrystalline	Type-B	Plg, Cpx, Ox, Ol, Opx, Amph	80/20	30	55	15		✓		2
NIS 436c	Nikia - main road	36°34′47.52″N	27°11′16.38″E	421	9	Diluted PDC	Crystal rich clast	4–5 cm	vesicular, aphyric/microcrystalline	Type-B	Plg, Cpx, Ox, Ol, Opx, Amph	70/30	40	53	7		✓	✓	
NIS 436d	Nikia - main road	36°34′47.52″N	27°11′16.38″E	421	9	Diluted PDC	Crystal rich clast		low vesicular, aphyric/microcrystalline	Type-A	Plg, Cpx, Ox, Ol, Opx, Amph	90/10	35	50	15		✓	✓	2

*Samples with mingling features are doubled to describe crystal-rich portions and pumiceous portions; "-" thin secrtion not available

CRC: Crystal-rich Clast; Plg: plagioclase; Cpx: clinopyroxene; Opx: orthopyroxene; Amph: amphibole; Ol: olivine; Ox: oxides; ph: phenocrysts (crystals >0.5 mm); mph: microphenocrysts (crystals >0.3 mm). Reaction rims: presence of olivines and/or opx with reaction rims to amphiboles; ph+mph in CRC (%): estimated abundance of crystals coarser than the average size of the microcrystalline groundmass in the CRCs.

Fig. 1. Location of the collected samples.

Crystal-rich clasts are highly heterogeneous in textures and were subdivided in three groups, named Type-A, Type-B and Type-C. The paragenesis is similar between the three groups: plagioclase represents more than 50% of the mineral assemblage, followed by amphibole and pyroxenes; olivine is rare; accessories phases are oxides and apatite. Amphibole can be found associated with plagioclase to form the microcrystalline groundmass network, either with acicular or tabular habitus, or as reaction rims on pyroxenes. Rare amphibole and pyroxene phenocrysts can be up to 2 mm, while plagioclase phenocrysts can reach 6 mm.

Type-A clasts are mostly found in fallout deposits and are characterised by microcrystalline texture with almost equigranular crystal size (0.1–0.5 mm), constituted by tabular plagioclases, amphiboles and pyroxenes (mainly orthopyroxene), with variable oxides content. Crystals are dispersed in a glassy, highly vesiculated groundmass, without a defined fabric.

Type-B clasts are the more variable in terms of crystal content and size; they show microcrystalline, inequigranular, low porphyritic texture, with variable crystal orientation defining at places a sort of network, likely the Type-C textures. They are present both in the fallout and lag-breccia deposits.

Type-C clasts are mostly found in the lag-breccia deposits, and they are characterized by a equigranular, low porphyritic textures with diktytaxitic voids, formed by a network of acicular plagioclases and amphiboles, with interstitial pyroxene. They show interstitial glass and variable vesicle abundance, generally lower than the other two types.

1.3. Geochemistry

The following table (Table 2) reports the complete dataset of major and trace element data on 31 whole-rock samples of pumice and CRCs of the Upper Pumice activity. Selected incompat-

Please cite this article as: F. Mastroianni, E. Braschi and M. Casalini et al., Data on unveiling the occurrence of transient, multi-contaminated mafic magmas inside a rhyolitic reservoir feeding an explosive eruption (Nisyros, Greece), Data in Brief, https://doi.org/10.1016/j.dib.2022.108077

Table 2

Major and trace element composition and Sr-Nd isotopic ratios of the studied samples from the Upper Pumice deposit (Nisyros, Greece). *Footnotes*: Major and trace elements data were performed at the Actalbs Laboratory (Ancaster-Ontario, Canada). Sr Isotope ratios were determined by TIMS Thermo-Finnigan Triton-Ti at the Radiogenic Isotope Laboratory of the Department of Earth Sciences, University of Florence. Nd isotope data were performed at the Radiogenic Isotope Laboratory of the IGG-CNR of Pisa by MC-ICPMS Thermo-Finnigan Neptune-Ti. * Major elements were analysed at the Department of Earth Sciences of the University Florence by XRF and trace elements were analysed at the Department of Earth Sciences of the University of Perugia by ICP-MS (see [8] for analytical details). Italic labels: trace elements analysed by XRF at the Department of Eearth Sciences of the University of Florence (see [6] for analytical details). La/Sm and Tb/Yb ratios are normalised to chondritic values. nd= not determined; bdl= below detection limit; 2se: 2 standard error of the mean.

Outcrop	8	8	8	5	5	5	5	1	1	1	1	1	1	2	2	3
Depositional unit	Lag-breccia	Lag-breccia	Lag-breccia	Fallout	Fallout	Fallout	Fallout	Fallout (U-A)	Fallout	Fallout	Fallout	Fallout	Fallout	Fallout	Fallout	Fallout
Lithology	CRC	CRC	CRC	Pumice	CRC	CRC	CRC	Pumice	CRC	CRC	CRC	CRC	CRC	CRC	CRC	Pumice
Texture	Type-C	Type-C	Type-B	Porphyritic	Type-A	Type-A	Type-A	Porphyritic	Type-A	Type-B	Type-A	Type-A	Type-B	Type-A	Type-A	Porphyritic
Sample	NIS312*	NIS313*	NIS314*	NIS315*	NIS316a*	NIS316b*	NIS316c*	NIS 353	NIS 356	NIS 357	NIS 358	NIS 359	NIS 360	NIS 370	NIS 371	NIS 374
Major Elements wt% (water free)																
SiO_2	56.74	56.45	57.33	71.43	62.04	60.15	64.17	70.58	57.87	58.17	60.69	62.72	57.61	64.14	59.27	71.66
TiO_2	0.61	0.71	0.69	0.31	0.57	0.65	0.73	0.36	0.93	0.67	0.69	0.76	0.64	0.84	0.61	0.33
Al_2O_3	19.22	19.30	18.41	14.41	16.71	18.27	16.78	15.13	18.10	18.32	17.95	16.90	18.43	16.41	17.03	14.28
FeO*	5.64	5.86	5.59	2.35	4.73	5.72	4.50	2.49	5.87	5.50	5.01	5.01	5.35	4.76	5.18	2.42
MnO	0.10	0.10	0.11	0.06	0.09	0.10	0.08	0.07	0.11	0.10	0.09	0.10	0.10	0.09	0.09	0.07
MgO	4.73	4.55	4.51	1.06	3.68	2.15	2.17	0.99	4.04	4.38	3.25	2.43	4.70	2.05	4.65	0.86
CaO	8.88	8.48	8.51	2.62	6.80	8.61	5.05	2.93	8.09	8.58	6.88	5.76	8.78	5.21	8.63	2.76
Na_2O	2.86	3.30	3.34	4.51	3.39	2.68	4.18	4.13	3.37	2.88	3.54	3.88	2.89	4.05	2.97	4.27
K_2O	1.12	1.12	1.38	3.20	1.89	1.55	2.16	3.23	1.48	1.31	1.82	2.25	1.40	2.29	1.46	3.26
P_2O_5	0.10	0.13	0.13	0.06	0.10	0.12	0.18	0.08	0.14	0.08	0.08	0.19	0.10	0.16	0.09	0.08
Total	100.00	100.00	100.00	100.00	100.00	100.00	100.00	100.00	100.00	100.00	100.00	100.00	100.00	100.00	100.00	100.00
LOI	0.58	0.78	0.71	3.05	1.83	1.34	1.77	3.25	1.60	1.63	2.08	2.07	1.66	2.21	1.58	2.74
Trace Elements (ppm)																
Be	nd	nd	nd	nd	nd	nd	nd	2	1	1	1	2	1	2	1	2
Sc	nd	nd	nd	nd	nd	nd	nd	5	20	19	15	11	19	12	19	4
V	*144*	143	*136*	31	107	*121*	*93*	39	167	146	136	90	140	98	130	35
Cr	*9.4*	5.8	*3.6*	3.4	18.0	*11.9*	*9.3*	bdl	bdl	bdl	bdl	bdl	bdl	bdl	20.0	bdl
Co	*22.4*	22.4	*20.6*	4.4	17.5	*19.7*	*10.5*	4	17	17	14	11	18	10	17	4
Ni	*3.29*	4.56	*4.19*	0.84	7.76	*5.85*	*1.27*	bdl	bdl	bdl	bdl	bdl	bdl	bdl	bdl	bdl
Cu	nd	bdl	nd	bdl	bdl	nd	nd	bdl	10	bdl	20	bdl	bdl	bdl	10	bdl
Zn	nd	bdl	nd	bdl	bdl	nd	nd	40	70	50	50	60	50	50	50	40
Ga	nd	13.8	nd	19	12.45	nd	nd	13	16	14	15	15	15	16	14	13
Rb	*34.6*	38.0	*42.2*	89.0	15.7	*45.5*	*38.8*	85	30	23	42	52	27	61	28	87
Sr	*571*	630	*606*	262	439	*552*	*379*	286	544	555	491	403	587	364	549	266
Y	*10.7*	13.7	*12.5*	19.0	18.1	*13.6*	*25.3*	17.2	22.9	16.4	17.4	20.7	15.7	29.2	16.3	16.5
Zr	*114*	123	*126*	188	143	*129*	*217*	219	157	128	153	189	122	227	139	194
Nb	*7.0*	7.6	*8.4*	12.6	8.5	*7.5*	*14.1*	10.4	9.2	5.6	7.1	9.4	6.1	11.8	5.8	9.2
Cs	bdl	0.6	bdl	4.0	1.0	bdl	bdl	2.8	1	0.6	1.2	1.4	0.7	1.8	0.8	2.9
Ba	*212*	258	*276*	710	348	*286*	*463*	786	315	253	391	429	258	484	291	775
La	*13.6*	17.8	*17.7*	38.4	17.0	*13.6*	*28.8*	40.4	22.3	14.5	18.5	24.3	14.9	38.1	16.4	35.7
Ce	*36.4*	31.5	*33.0*	53.4	28.8	*30.8*	*50.3*	65.2	40.6	28.5	37.2	46	29.5	56.7	33.8	59.5
Pr	nd	4.0	nd	6	4.3	nd	nd	7.06	5.26	3.43	3.99	5.29	3.53	8.42	3.81	5.83
Nd	*18.3*	13.9	*14.9*	21.9	12.6	*16.0*	*21.7*	22.8	20.1	13.5	15.1	19.5	13.6	31.7	14.5	19
Sm	nd	3.6	nd	3.2	3.5	nd	nd	3.72	4.36	3.03	3.13	4.09	3.03	6.26	3.02	3.03
Eu	nd	1.1	nd	0.7	0.9	nd	nd	0.76	1.21	0.91	0.89	1.06	0.94	1.32	0.86	0.71
Gd	nd	3.7	nd	3.00	3.13	nd	nd	3.10	4.31	2.97	2.94	3.80	2.96	5.33	2.98	2.68
Tb	nd	0.6	nd	0.4	0.5	nd	nd	0.48	0.67	0.48	0.49	0.58	0.47	0.9	0.49	0.43
Dy	nd	3.5	nd	2.5	3.0	nd	nd	2.83	4.01	2.86	2.99	3.47	2.89	5.19	2.91	2.59
Ho	nd	0.7	nd	0.49	0.61	nd	nd	0.57	0.81	0.57	0.6	0.73	0.55	1.01	0.55	0.52

(*continued on next page*)

Table 2 (*continued*)

Outcrop	8	8	8	5	5	5	5	1	1	1	1	1	1	2	2	3
Depositional unit	Lag-breccia	Lag-breccia	Lag-breccia	Fallout	Fallout	Fallout	Fallout	Fallout (U-A)	Fallout	Fallout	Fallout	Fallout	Fallout	Fallout	Fallout	Fallout
Lithology	CRC	CRC	CRC	Pumice	CRC	CRC	CRC	Pumice	CRC	CRC	CRC	CRC	CRC	CRC	CRC	Pumice
Texture	Type-C	Type-C	Type-B	Porphyritic	Type-A	Type-A	Type-A	Porphyritic	Type-A	Type-B	Type-A	Type-A	Type-B	Type-A	Type-A	Porphyritic
Er	nd	1.9	nd	1.4	1.8	nd	nd	1.79	2.27	1.68	1.76	2.09	1.6	2.86	1.69	1.62
Tm	nd	0.27	nd	0.20	0.23	nd	nd	0.27	0.34	0.24	0.25	0.30	0.22	0.43	0.23	0.27
Yb	nd	1.9	nd	1.7	1.7	nd	nd	1.95	2.22	1.63	1.78	2.13	1.5	2.9	1.56	1.9
Lu	nd	0.30	nd	0.28	0.27	nd	nd	0.33	0.35	0.27	0.31	0.36	0.26	0.50	0.27	0.33
Hf	nd	3.6	nd	4.3	3.4	nd	nd	5.0	4.2	3.2	3.7	4.5	3.1	6.0	3.6	4.4
Ta	bdl	0.6	bdl	1.1	0.6	bdl	bdl	1.14	0.74	0.49	0.64	0.92	0.50	1.04	0.53	1.15
Pb	*6.0*	6.3	*6.9*	14.0	7.8	*11.6*	*11.0*	14	8	8	8	9	5	11	6	14
Th	*4.6*	2.7	*5.0*	13.0	8.6	*6.3*	*9.9*	11.9	4.42	3.19	4.76	5.94	3.13	7.52	3.96	11.4
U	nd	nd	nd	bdl	nd	nd	nd	3.44	1.17	0.86	1.27	1.6	0.84	1.94	1.04	3.31
Ratios																
Zr/Ba	0.54	0.48	0.46	0.26	0.41	0.45	0.47	0.28	0.50	0.51	0.39	0.44	0.47	0.47	0.48	0.25
Rb/Sr	0.06	0.06	0.07	0.34	0.04	0.08	0.10	0.30	0.06	0.04	0.09	0.13	0.05	0.17	0.05	0.33
Sr/Ba	2.69	2.45	2.20	0.37	1.26	1.93	0.82	0.36	1.73	2.19	1.26	0.94	2.28	0.75	1.89	0.34
La/SmN		3.47		8.40	3.42			7.60	3.58	3.35	4.14	4.16	3.44	4.26	3.80	8.25
Tb/YbN		1.23		0.96	1.22			1.00	1.23	1.20	1.12	1.11	1.28	1.27	1.28	0.92
Eu/Eu^*		0.98		0.72	0.91			0.71	0.90	0.98	0.94	0.86	1.01	0.73	0.92	0.79
Isotope ratios																
$^{87}Sr/^{86}Sr$	0.704342	0.704255	0.704202	0.704563	0.704478	0.704327	0.704754	0.704532	0.704595	0.704396	0.704441	0.704580	0.704313	0.704876	nd	nd
2se	0.000005	0.000007	0.000006	0.000006	0.000006	0.000007	0.000006	0.000005	0.000004	0.000005	0.000006	0.000006	0.000005	0.000006	nd	nd
$^{143}Nd/^{144}Nd$	0.512533	0.512591	0.512616	0.512615	0.512552	0.512558	0.512556	0.512611	0.512539	0.512531	0.512560	0.512566	0.512537	0.512537	nd	nd
2se	0.000005	0.000005	0.000006	0.000005	0.000004	0.000004	0.000012	0.000009	0.000009	0.000008	0.000003	0.000009	0.000008	0.000010	nd	nd
Outcrop	4	4	4	6	7a	8	8	8	8	8	8	8	8	9	9	
Depositional unit	Fallout	Fallout	Fallout	Fallout	Lag-breccia	Lag-breccia	Lag-breccia	Lag-breccia	Lag-breccia	Lag-breccia	Lag-breccia	Lag-breccia	Lag-breccia	Diluted PDC	Diluted PDC	
Lithology	Pumice	CRC	CRC	Pumice	CRC	Pumice	Pumice	CRC	CRC	CRC	CRC	CRC	CRC	Pumice	Pumice	
Texture	Porphyritic	Type-A	Type-A	Porphyritic	Type-C	Porphyritic	Porphyritic	Type-C	Type-B	Type-B	Type-C	Type-C	Type-C	Porphyritic	Porphyritic	
Sample	NIS 377	NIS 378	NIS 381	NIS 401	NIS 416	NIS 418	NIS 419	NIS 421	NIS 423	NIS 424	NIS 425	NIS 426	NIS 427	NIS 431	NIS 433	
Major Elements wt% (water free)																
SiO_2	69.05	60.84	59.05	71.11	58.99	71.22	71.27	59.63	58.65	56.65	57.42	57.17	57.44	70.97	71.04	
TiO_2	0.36	0.63	1.01	0.35	0.66	0.34	0.34	0.66	0.72	0.75	0.65	0.72	0.64	0.34	0.34	
Al_2O_3	14.83	16.33	16.68	14.59	17.84	14.46	14.70	18.09	17.88	18.53	17.61	17.81	17.49	14.93	14.87	
FeO^*	2.70	4.79	5.93	2.47	5.51	2.39	2.40	5.26	5.15	5.76	5.48	5.53	5.53	2.40	2.40	
MnO	0.07	0.09	0.11	0.07	0.10	0.07	0.07	0.11	0.10	0.11	0.10	0.10	0.10	0.07	0.07	
MgO	1.55	4.47	3.37	0.98	4.22	0.90	0.87	3.54	4.39	4.56	5.20	5.14	5.15	0.87	0.82	
CaO	3.27	8.02	7.17	2.92	8.28	2.83	2.78	7.29	8.56	8.95	9.36	9.42	9.60	2.79	2.80	
Na_2O	5.01	3.07	4.81	4.19	2.94	4.26	4.19	3.74	3.09	3.24	2.98	2.81	2.77	4.33	4.37	
K_2O	3.05	1.63	1.68	3.24	1.33	3.44	3.27	1.57	1.33	1.31	1.08	1.17	1.17	3.23	3.21	
P_2O_5	0.11	0.12	0.19	0.08	0.13	0.08	0.09	0.12	0.12	0.13	0.11	0.13	0.10	0.07	0.08	
Total	100.00	100.00	100.00	100.00	100.00	100.00	100.00	100.00	100.00	100.00	100.00	100.00	100.00	100.00	100.00	
LOI	5.29	1.89	3.44	3.14	1.41	2.35	2.24	1.42	1.42	1.33	1.07	1.33	1.33	2.43	2.38	
Trace Elements (ppm)																
Be	2	1	1	2	1	2	2	1	1	1	1	1	1	2	2	
Sc	5	18	17	4	16	4	4	17	19	17	22	22	24	4	4	
V	39	121	152	36	137	36	34	149	122	145	148	153	158	36	35	
Cr	bdl	40.0	bdl	bdl	bdl	bdl	bdl	bdl	bdl	bdl	30.0	bdl	bdl	bdl	bdl	
Co	5	16	13	4	17	4	4	15	15	19	19	19	19	4	4	
Ni	bdl	bdl	bdl	bdl	bdl	bdl	bdl	bdl	bdl	bdl	bdl	bdl	bdl	bdl	bdl	

(*continued on next page*)

Please cite this article as: F. Mastroianni, E. Braschi and M. Casalini et al., Data on unveiling the occurrence of transient, multi-contaminated mafic magmas inside a rhyolitic reservoir feeding an explosive eruption (Nisyros, Greece), Data in Brief, https://doi.org/10.1016/j.dib.2022.108077

Table 2 (*continued*)

Outcrop	8	8	8	5	5	5	5	1	1	1	1	1	1	2	2	3
Depositional unit	Lag-breccia	Lag-breccia	Lag-breccia	Fallout	Fallout	Fallout	Fallout	Fallout (U-A)	Fallout	Fallout	Fallout	Fallout	Fallout	Fallout	Fallout	Fallout
Lithology	CRC	CRC	CRC	Pumice	CRC	CRC	CRC	Pumice	CRC	CRC	CRC	CRC	CRC	CRC	CRC	Pumice
Texture	Type-C	Type-C	Type-B	Porphyritic	Type-A	Type-A	Type-A	Porphyritic	Type-A	Type-B	Type-A	Type-A	Type-B	Type-A	Type-A	Porphyritic
Cu	bdl	bdl	bdl	bdl	bdl	10	10	bdl	bdl	10	bdl	bdl	bdl	bdl	bdl	
Zn	70	50	60	40	50	30	40	50	50	50	50	50	50	40	40	
Ga	12	14	15	13	15	13	13	15	14	15	14	14	14	13	13	
Rb	80	37	38	86	24	88	88	40	29	30	24	20	25	87	90	
Sr	303	467	419	280	607	276	277	519	552	639	598	595	504	277	278	
Y	17	16.8	24.6	17.3	15.7	16.4	17.4	18.2	16.2	17.3	15.9	16	16.6	15.7	15.8	
Zr	174	143	197	203	123	200	189	117	139	130	115	116	113	199	190	
Nb	8.9	6.9	10.6	9.9	6.0	9.3	9.4	5.5	7.1	7.0	5.6	6.0	5.2	9.5	9.6	
Cs	2.6	1.0	1.3	2.8	0.6	2.8	2.9	1.1	0.8	0.7	0.5	0.5	0.6	2.8	2.9	
Ba	690	330	332	761	265	780	797	423	294	284	237	234	227	779	798	
La	33	19	22.7	35.9	15.7	34.3	34.4	18.4	16.4	16.8	13.7	13.8	13.4	33.8	34.4	
Ce	56.8	36.3	45.8	57.7	31.3	58	57.9	34.9	33.3	32.8	27.6	27.8	26.7	57.4	57.9	
Pr	5.58	3.96	5.28	5.94	3.65	5.52	5.7	3.93	3.7	3.81	3.21	3.29	3.21	5.46	5.56	
Nd	18.1	15.4	20.7	19.6	14.4	18.1	18.7	15	13.7	15.3	12.9	13.4	12.6	18	18	
Sm	3.15	3.15	4.5	3.34	3.01	3.06	3.11	3.1	2.99	3.29	2.89	3.04	2.76	2.84	2.93	
Eu	0.71	0.86	1.22	0.73	0.92	0.69	0.74	0.95	0.87	0.98	0.90	0.88	0.89	0.65	0.67	
Gd	2.77	3.01	4.44	2.76	2.93	2.56	2.76	3.05	2.87	3.21	2.88	3.14	2.95	2.44	2.57	
Tb	0.44	0.5	0.7	0.45	0.47	0.42	0.45	0.49	0.47	0.53	0.45	0.49	0.49	0.4	0.4	
Dy	2.71	2.95	4.32	2.8	2.79	2.5	2.7	3.04	2.85	3.04	2.69	2.71	2.95	2.49	2.55	
Ho	0.54	0.59	0.85	0.55	0.56	0.55	0.55	0.63	0.55	0.59	0.55	0.56	0.58	0.52	0.52	
Er	1.75	1.73	2.4	1.69	1.56	1.6	1.81	1.86	1.61	1.77	1.56	1.58	1.77	1.61	1.61	
Tm	0.28	0.25	0.38	0.27	0.24	0.26	0.27	0.28	0.24	0.26	0.23	0.24	0.24	0.26	0.25	
Yb	1.93	1.75	2.46	1.91	1.59	1.85	1.95	1.75	1.63	1.71	1.49	1.53	1.6	1.92	1.82	
Lu	0.33	0.29	0.39	0.33	0.25	0.33	0.33	0.30	0.27	0.26	0.24	0.24	0.28	0.34	0.32	
Hf	4.3	3.6	4.9	5.0	3.3	4.7	4.5	3	3.4	3.2	3.1	3.2	3	4.6	4.3	
Ta	1.07	0.58	0.9	1.13	0.51	1.13	1.12	0.49	0.64	0.59	0.48	0.50	0.44	1.14	1.11	
Pb	13	7	8	14	bdl	14	13	8	6	bdl	bdl	6	6	15	14	
Th	10.4	4.64	5.06	11.1	3.19	11	11	3.36	3.94	3.35	2.67	2.73	2.94	10.7	11	
U	3.06	1.29	1.38	3.33	0.89	3.32	3.34	0.95	1.05	0.92	0.71	0.72	0.73	3.24	3.36	
Ratios																
Zr/Ba	0.25	0.43	0.59	0.27	0.46	0.26	0.24	0.28	0.47	0.46	0.49	0.50	0.50	0.26	0.24	
Rb/Sr	0.26	0.08	0.09	0.31	0.04	0.32	0.32	0.08	0.05	0.05	0.04	0.03	0.05	0.31	0.32	
Sr/Ba	0.44	1.42	1.26	0.37	2.29	0.35	0.35	1.23	1.88	2.25	2.52	2.54	2.22	0.36	0.35	
La/SmN	7.33	4.22	3.53	7.52	3.65	7.85	7.74	4.15	3.84	3.57	3.32	3.18	3.40	8.33	8.22	
Tb/YbN	0.93	1.17	1.16	0.96	1.21	0.93	0.94	1.14	1.18	1.27	1.23	1.31	1.25	0.85	0.90	
Eu/Eu*	0.77	0.89	0.88	0.76	1.00	0.78	0.81	1.00	0.96	0.97	1.00	0.92	1.00	0.78	0.77	
Isotope ratios																
$^{87}Sr/^{86}Sr$	0.704520	0.704538	nd	nd	0.704256	nd	0.704526	0.704688	0.704551	nd	nd	0.704302	0.704484	nd	nd	
2se	0.000005	0.000005	nd	nd	0.000006	nd	0.000004	0.000006	0.000005	nd	nd	0.000006	0.000007	nd	nd	
$^{143}Nd/^{144}Nd$	0.512610	0.512517	nd	nd	0.512545	nd	0.512622	0.512616	0.512506	nd	nd	0.512548	0.512534	nd	nd	
2se	0.000007	0.000008	nd	nd	0.000008	nd	0.000007	0.000007	0.000009	nd	nd	0.000008	0.000008	nd	nd	

Major and trace elements data were performed at the Actalbs Laboratory (Ancaster-Ontario, Canada). Sr Isotope ratios were determined by TIMS Thermo-Finnigan Triton-Ti at the Radiogenic Isotope Laboratory of the Department of Earth Sciences, University of Florence. Nd isotope data were performed at the Radiogenic Isotope Laboratory of the IGG-CNR of Pisa by MC-ICPMS Thermo-Finnigan Neptune-Ti. * Major elements were analysed at the Department of Earth Sciences of the University Florence by XRF and trace elements were analysed at the Department of Earth Sciences of the University of Perugia by ICP-MS (see [6] for analytical details). Italic labels: trace elements analysed by XRF at the Department of Eearth Sciences of the University of Florence (see [6] for analytical details). La/Sm and Tb/Yb ratios are normalised to chondritic values. nd= not determined; bdl= below detection limit; 2se: 2 standard error of the mean.

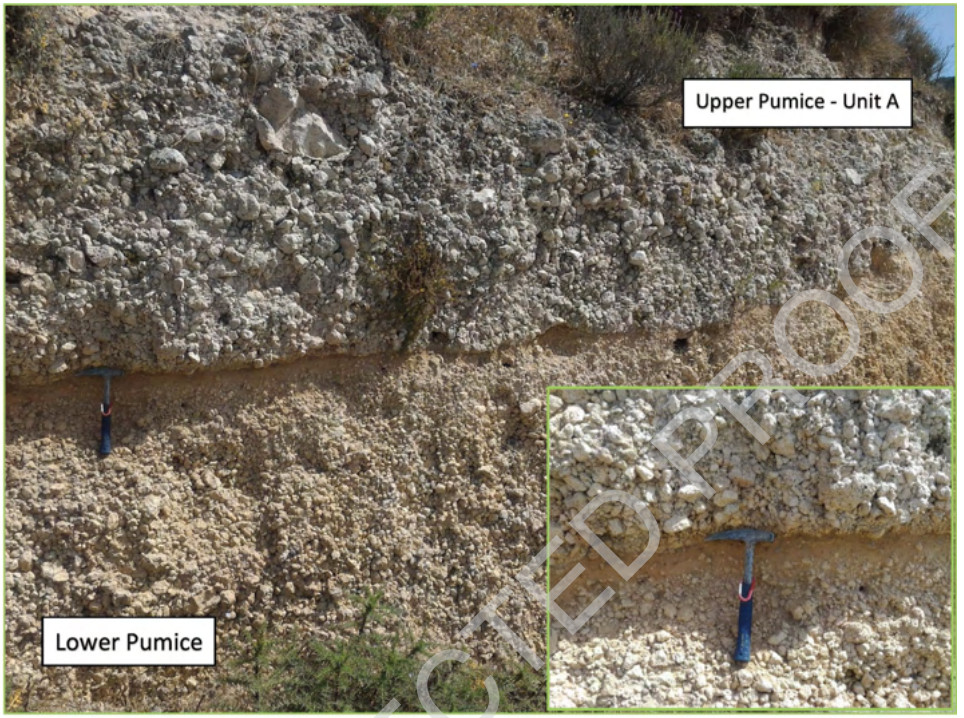

Fig. 2. Images of the paleosoil horizon marking the base of the UP pyroclastic sequence (a detail is showed in the inset) and the contact with the deposit of the previous Lower Pumice (LP) explosive eruption.

ible trace elements and Rare Earth Elements (REE) together with Sr-Nd isotope ratios were also determined on a further selection of 22 samples.

The pumices are rhyolites (SiO_2 >70 wt.%) belonging to the high-K calc-alkaline series, whereas the CRC show an affinity with the calc-alkaline series, ranging from basaltic andesite/andesite to dacite (SiO_2 between 56 and 64 wt.%). Loss on ignition (LOI) is always lower than 2% in the CRCs, while it is up to 5.3% in the pumices.

REE and incompatible element patterns (Figs. 23 and 24) are typical for subduction-related calc-alkaline rocks. REE values are normalised to the chondrite data, while incompatible elements are normalised to the primordial mantle values [9]. Symbols used in the graphs are the same used in Braschi et al. [1]: purple symbols represent samples from the fallout deposit, the green ones are samples from the lag-breccia deposit and those from PDC units are black; open diamonds represent pumices, CRCs have different symbols for each texture typology (circles for Type-A, triangles for Type-B and squares for Type-C).

Please cite this article as: F. Mastroianni, E. Braschi and M. Casalini et al., Data on unveiling the occurrence of transient, multi-contaminated mafic magmas inside a rhyolitic reservoir feeding an explosive eruption (Nisyros, Greece), Data in Brief, https://doi.org/10.1016/j.dib.2022.108077

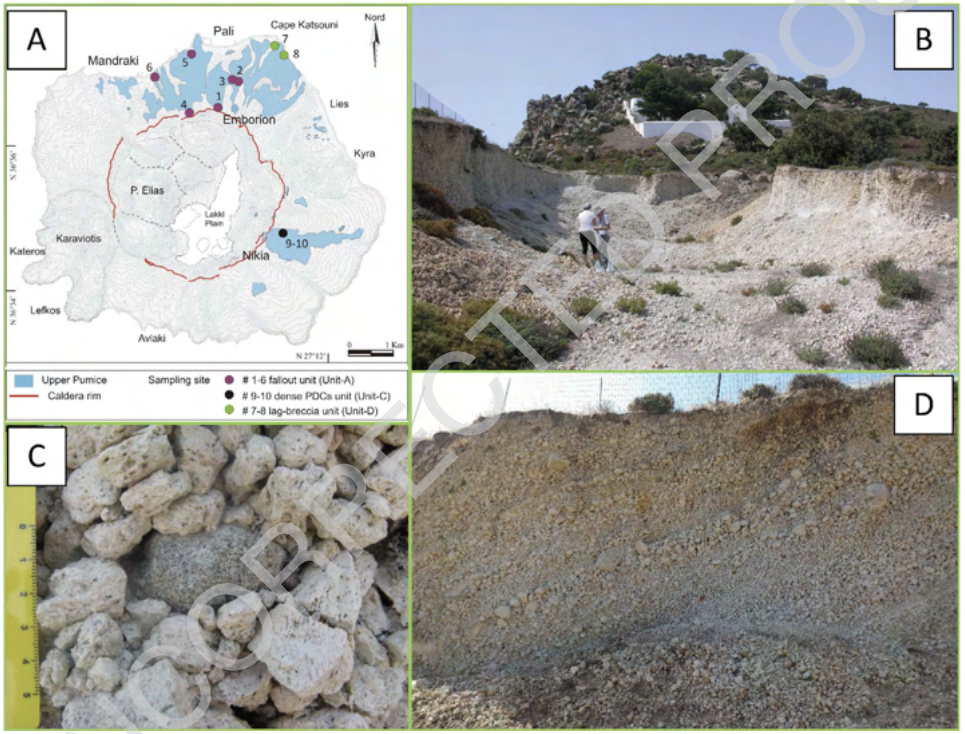

Fig. 3. Selection of representative images of the basal fallout unit (Unit-A) outcropping in the northern part of the caldera rim (outcrop 1) near the Emborion village. (A) schematic map of the UP distribution together with the location of the different sampling site (see legend for detail); (B) main view of the outcrop 1. The Unit-A consists in a 0.5 to 8 m thick level of unconsolidated, granular sustained, moderately assorted, massive fallout, mainly composed of white sub-angular pumices, with size varying from lapilli to small blocks and dense Crystal-rich Clasts (CRC) (C). Occasional evident stratification, formed by layers of clasts at different grain size, is observed (D) and interpreted as the result of syn-depositional reworking in the most proximal deposits [2–4].

Please cite this article as: F. Mastroianni, E. Braschi and M. Casalini et al., Data on unveiling the occurrence of transient, multi-contaminated mafic magmas inside a rhyolitic reservoir feeding an explosive eruption (Nisyros, Greece), Data in Brief, https://doi.org/10.1016/j.dib.2022.108077

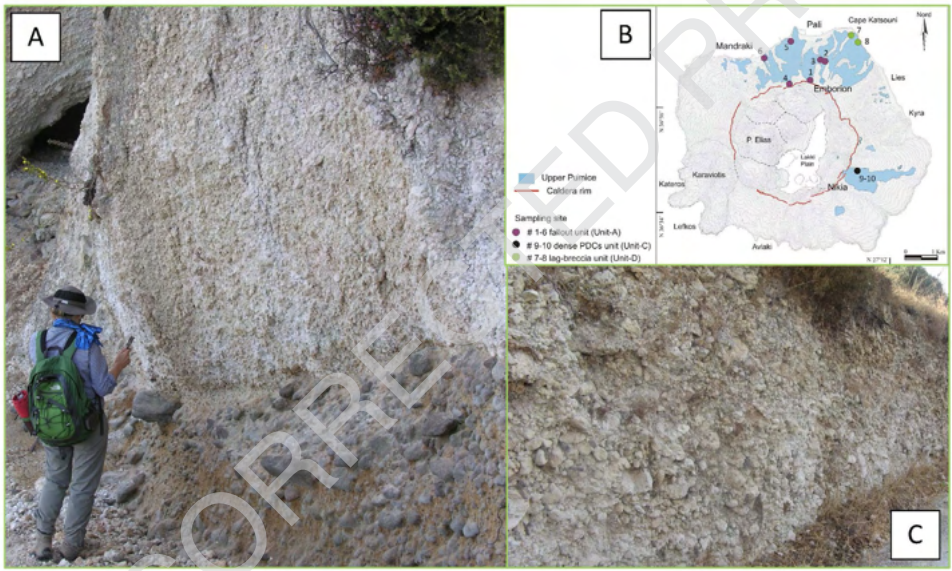

Fig. 4. Representative images of the basal fallout unit (Unit-A) outcropping in the northern part of the caldera, just inside the rim border (outcrop 4) (A) and along the main road, near the coast above Pali village (outcrop 5) (C). Pumices are the prevalent juvenile components whereas CRCs constitute about 5% of the deposit. The lithic content is less than 2%, there are very small quantities of fine ash and loose crystals as matrix. This unit has been interpreted as pyroclastic fall deposit, emplaced from the column of a Plinian or sub-Plinian eruption [2,3,5]. The schematic map of the UP distribution and outcrops location is also reported (B).

Please cite this article as: F. Mastroianni, E. Braschi and M. Casalini et al., Data on unveiling the occurrence of transient, multi-contaminated mafic magmas inside a rhyolitic reservoir feeding an explosive eruption (Nisyros, Greece), Data in Brief, https://doi.org/10.1016/j.dib.2022.108077

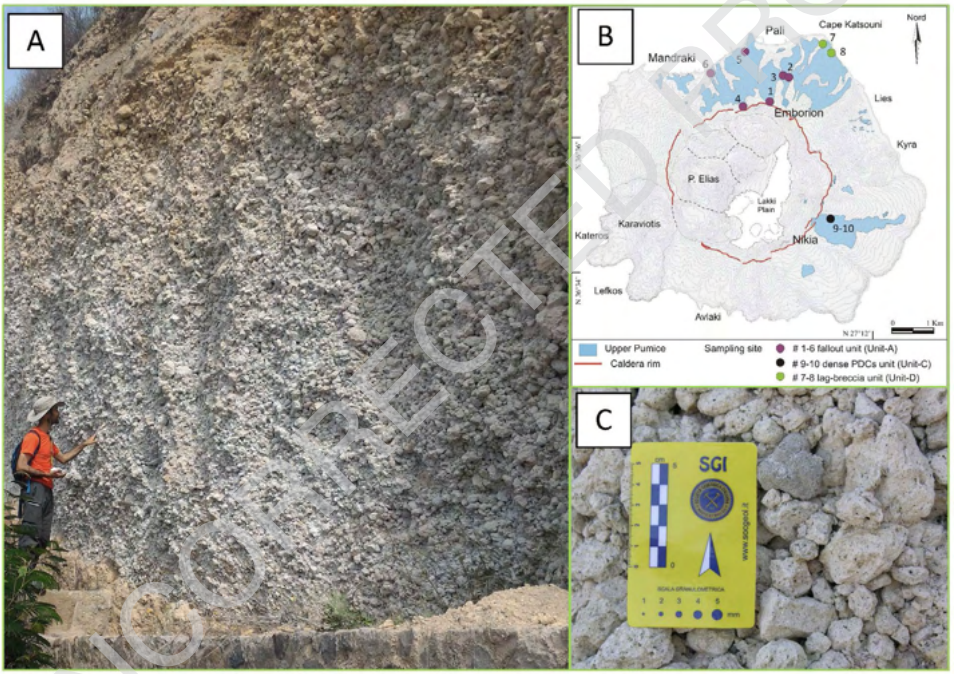

Fig. 5. Representative image of outcrop 6 where the fallout unit is particularly well preserved (A). CRCs clasts are evident within the pumices showing grey colour and globular shapes (C). The schematic map of the UP distribution and outcrops location is also reported (B) (For interpretation of the references to colour in this figure legend, the reader is referred to the web version of this article).

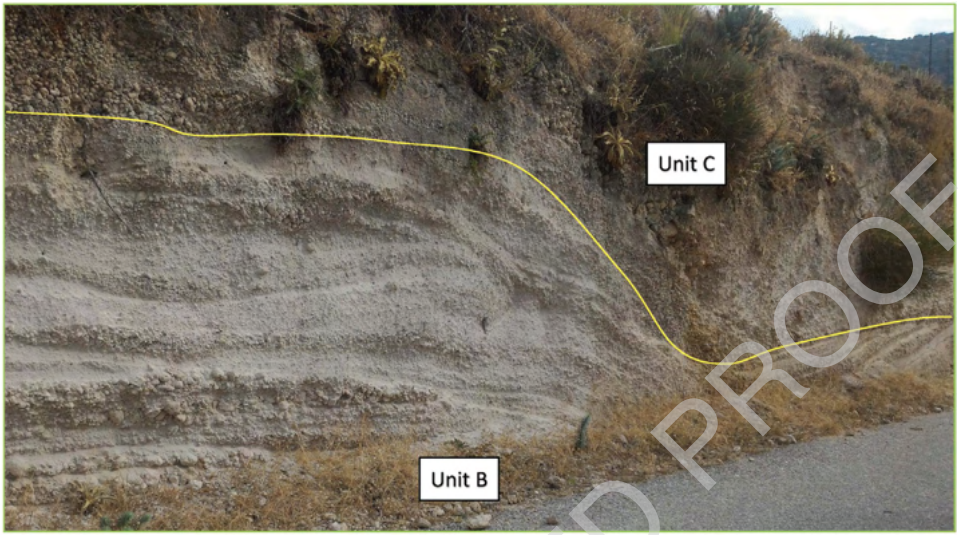

Fig. 6. Representative image of the second unit (Unit-B) at the contact with the overlying Unit-C, close to outcrop 7, along the main road to Cape Katsouni, in the north-east part of Nisyros. Unit-B is a succession of several layers of fully diluted pyroclastic current (according to [6]) alternated with fallout levels. The flow levels are formed by a matrix of ash and loose crystals where sub- to well-rounded pumice lapilli are immersed, alternating with layers of coarser ash. Unit-C is a massive deposit of unconsolidated material, composed of coarse ash, fine lapilli and loose crystals, with well rounded, slightly vesiculated pumice and dispersed lithic clasts [2], interpreted as a granular fluid-based current (according to [6]).

Fig. 7. Representative image of the principal outcrop of unit-D exposed on the main street south of Cape Katsouni (outcrop 8). Unit-D is a dense pyroclastic current, gradually interlayered toward the top with lithic-rich lenses. This unit is constituted by a breccia deposit composed of rounded pumices and abundant (up to 15%) dense juvenile clasts with crenulated or "bread crust" surfaces, up to few tens of centimetres in diameter, and angular lithic clasts within an unconsolidated ash matrix including. Lithics mainly consist of fresh and hydrothermalised lava clasts; fragments of hypoabyssal igneous rocks, skarn and limestone with hydrothermal alteration are also present [as also reported by 2, 3]. Unit-D is interpreted as a lag-breccia deposit [2], emplaced from a dense PDC formed by the collapse of the eruptive column as a consequence of the caldera collapse [7].

Please cite this article as: F. Mastroianni, E. Braschi and M. Casalini et al., Data on unveiling the occurrence of transient, multi-contaminated mafic magmas inside a rhyolitic reservoir feeding an explosive eruption (Nisyros, Greece), Data in Brief, https://doi.org/10.1016/j.dib.2022.108077

Fig. 8. Image of the top unit of the UP sequence (Unit-E) composed by a massive or weakly laminated deposit formed by grey ash with loose crystals, rounded centimetre-sized pumice and lithic lava and limestone clasts (about 20%, [2]). This unit have been interpreted as a deposit from diluted pyroclastic density currents [2] or due to a phreatomagmatic eruptive event [5].

Please cite this article as: F. Mastroianni, E. Braschi and M. Casalini et al., Data on unveiling the occurrence of transient, multi-contaminated mafic magmas inside a rhyolitic reservoir feeding an explosive eruption (Nisyros, Greece), Data in Brief, https://doi.org/10.1016/j.dib.2022.108077

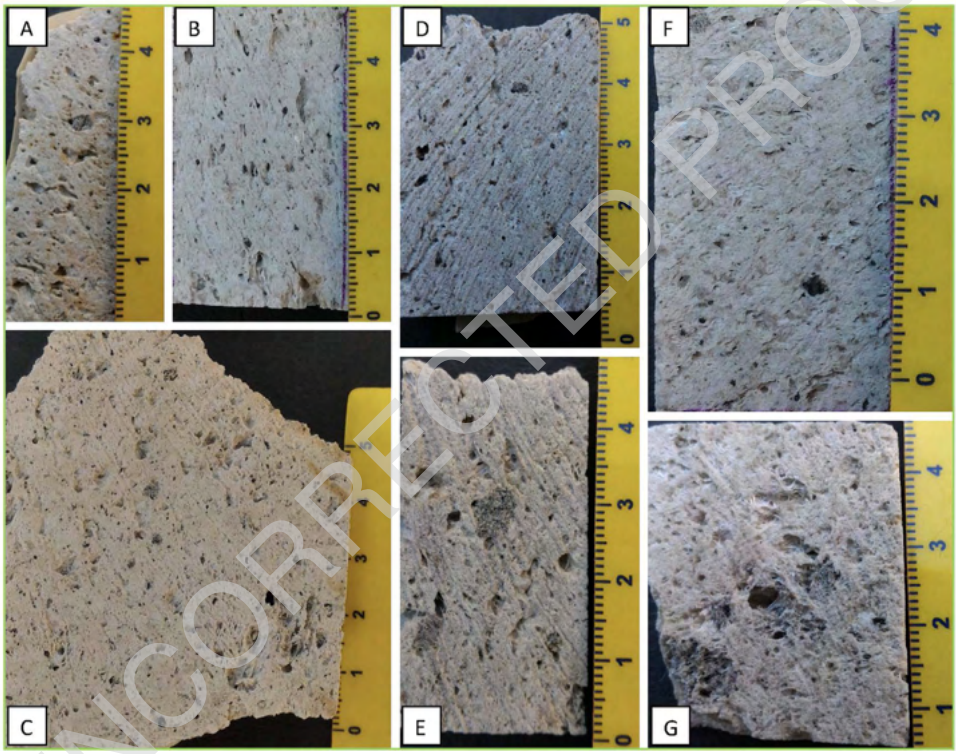

Fig. 9. Cut blocks of pumice samples collected in different outcrops from the fallout deposit (A: NIS353; B: NIS374; C: NIS377) and from the lag-breccia deposit (D: NIS418; E: NIS419, outcrop 8). Pumices from the PDC deposits collected in outcrop 9 are also shown (F: NIS431; G: NIS433). Pumice clasts are white or pale yellow in colour, porphyritic and highly vesiculated, sub-angular, and range from 10 to 40 cm in diameter. Pumices often include micro-enclaves or grey bands (E, F) (For interpretation of the references to colour in this figure legend, the reader is referred to the web version of this article).

Please cite this article as: F. Mastroianni, E. Braschi and M. Casalini et al., Data on unveiling the occurrence of transient, multi-contaminated mafic magmas inside a rhyolitic reservoir feeding an explosive eruption (Nisyros, Greece), Data in Brief, https://doi.org/10.1016/j.dib.2022.108077

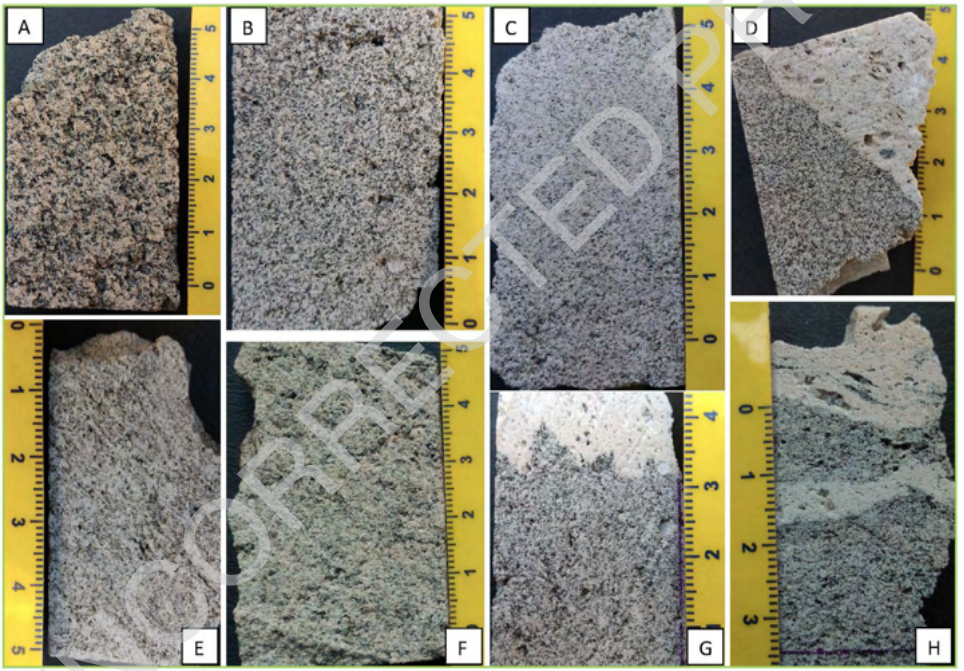

Fig. 10. Cut blocks of representative CRC samples of the collected from the fallout deposits. A: NIS356; B: NIS357; C: NIS359; D: NIS358; E: NIS370; F: NIS371; G: NIS378; H: NIS381. See Table 1 for details.

Please cite this article as: F. Mastroianni, E. Braschi and M. Casalini et al., Data on unveiling the occurrence of transient, multi-contaminated mafic magmas inside a rhyolitic reservoir feeding an explosive eruption (Nisyros, Greece), Data in Brief, https://doi.org/10.1016/j.dib.2022.108077

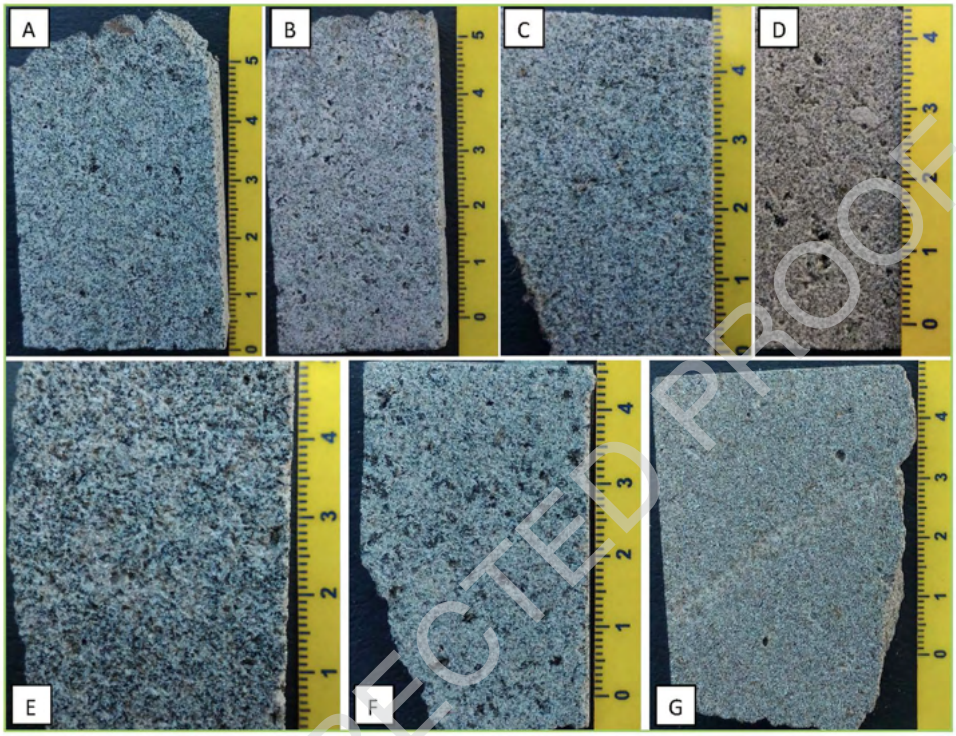

Fig. 11. Cut blocks of representative CRC samples collected from the lag-breccia deposits (outcrop 8). A: NIS426; B: NIS425; C: NIS423; D: NIS416; E: NIS424; F: NIS427; G: NIS421. See Table 1 for details.

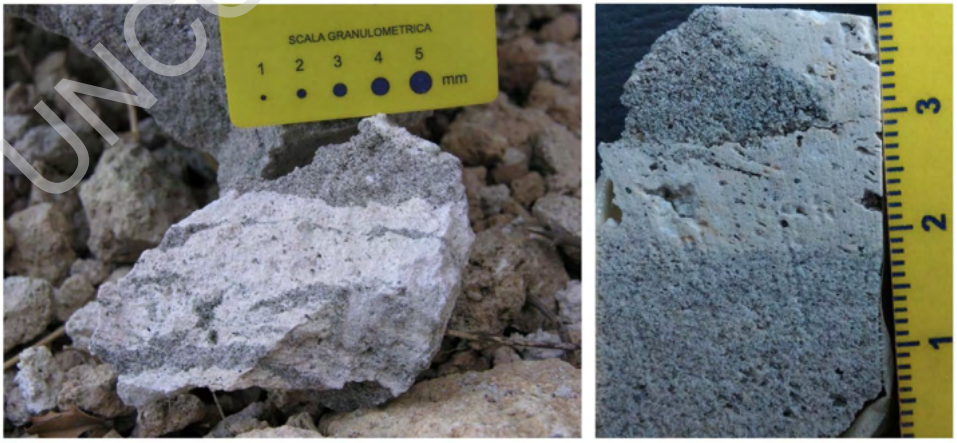

Fig. 12. Representative photos of two samples showing the contacts between pumice and CRCs. The contacte between the two lithologies are sharp but convoluted due to a process of plastic interaction.

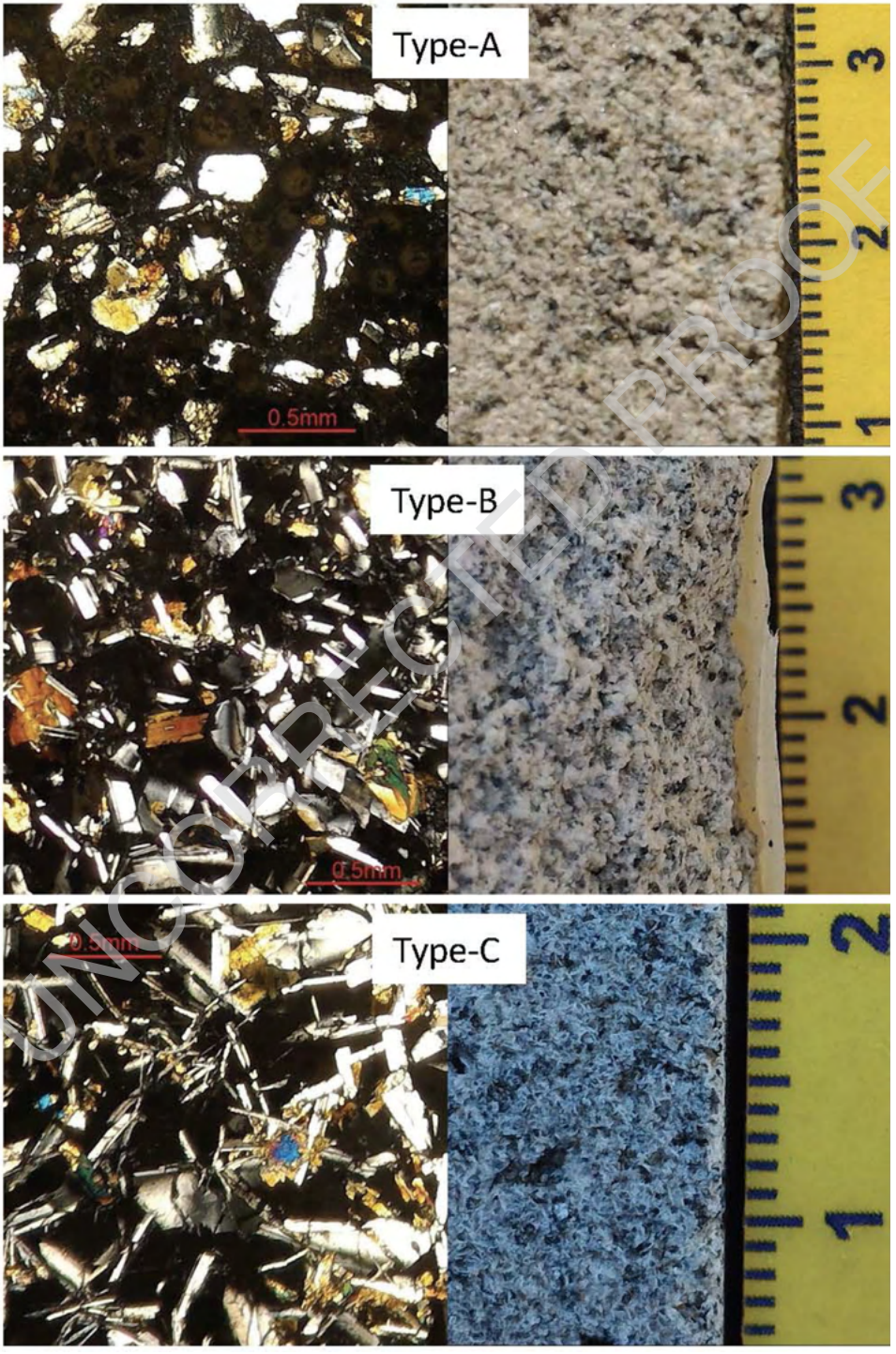

Fig. 13. Comparison between hand-specimen blocks and the relative microphotographs acquired on the thin section, showing the three different textures types defined among the CRC samples.

Please cite this article as: F. Mastroianni, E. Braschi and M. Casalini et al., Data on unveiling the occurrence of transient, multi-contaminated mafic magmas inside a rhyolitic reservoir feeding an explosive eruption (Nisyros, Greece), Data in Brief, https://doi.org/10.1016/j.dib.2022.108077

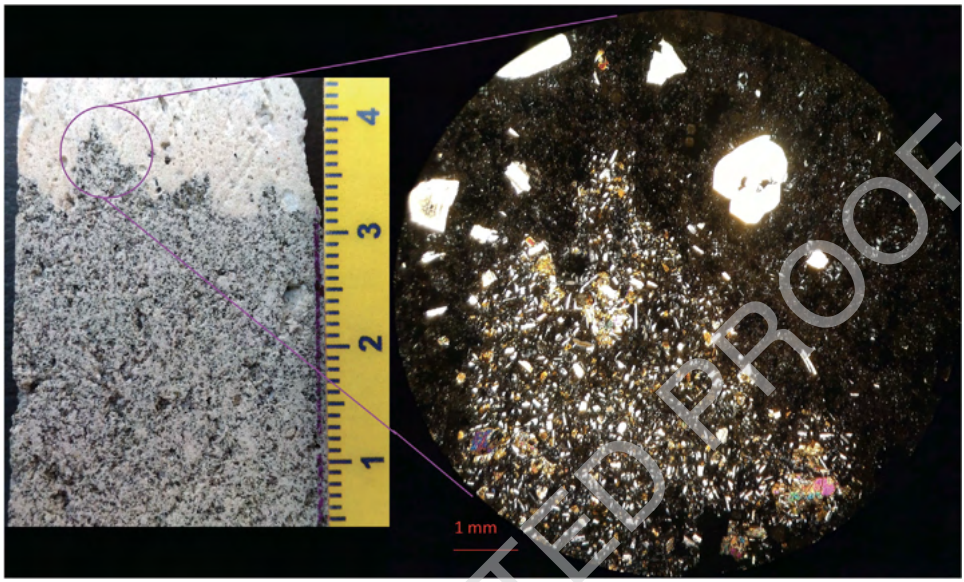

Fig. 14. Cut block sample and the relative microphotograph detail of the contact between pumices and a dense crystal-rich clast. The dispersion of CRC portions into the pumice is evident both as loose crystals and micro-encalves.

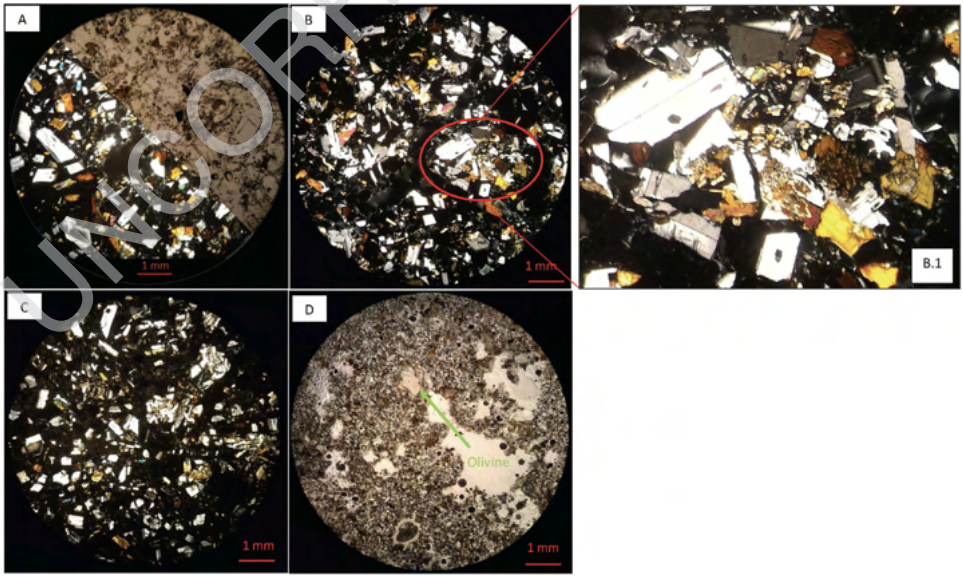

Fig. 15. Thin section microphotograph of Type-A CRCs. A: NIS356, parallel and crossed nicols; B: NIS 356, detail of crystal cloth (B.1); C: NIS 371; D: NIS 378 with a resorbed olivine phenocryst (parallel nicols).

Please cite this article as: F. Mastroianni, E. Braschi and M. Casalini et al., Data on unveiling the occurrence of transient, multi-contaminated mafic magmas inside a rhyolitic reservoir feeding an explosive eruption (Nisyros, Greece), Data in Brief, https://doi.org/10.1016/j.dib.2022.108077

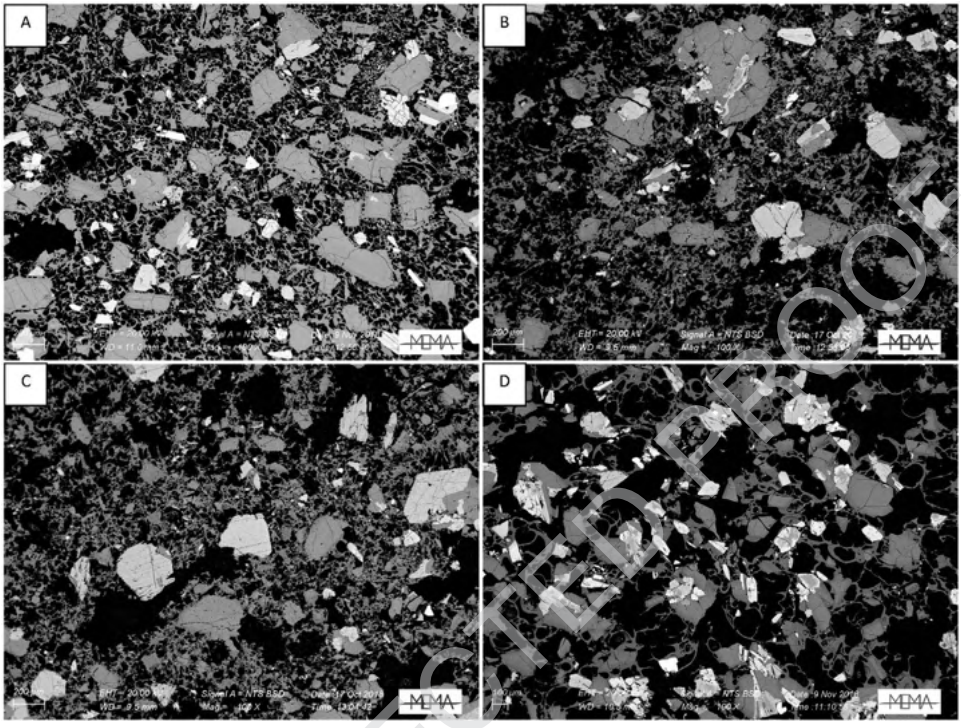

Fig. 16. BSE images of Type-A CRC obtained by SEM. A: NIS317; B and C: NIS368d; D: NIS420.

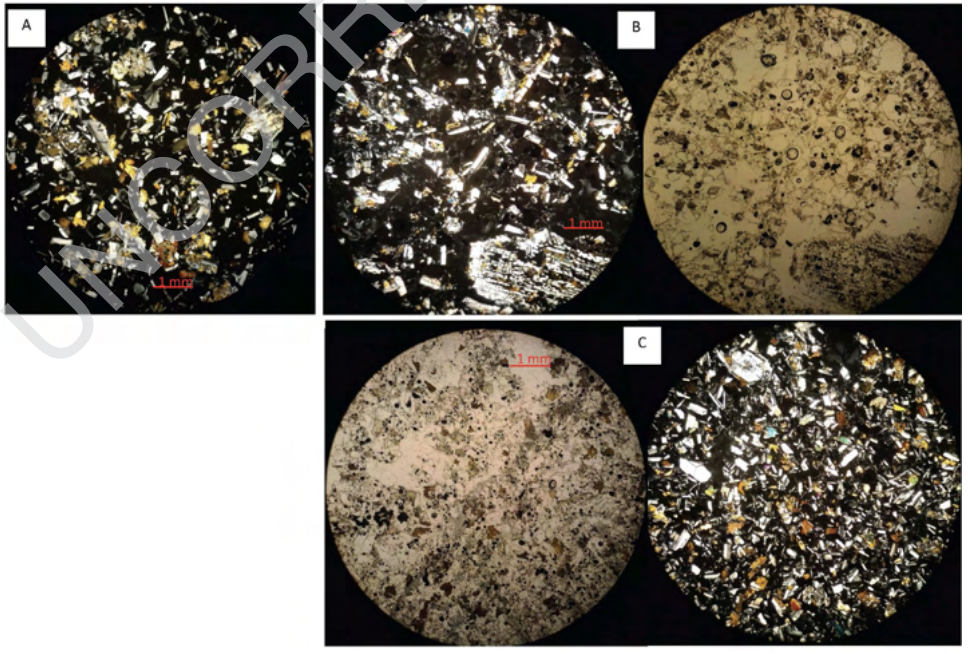

Fig. 17. Thin section microphotograph of Type-B CRCs. A: NIS314, crystal-cloth presence; B: NIS423, parallel and crossed nicols, plagioclase phenocryst with sieved texture; C: NIS360, parallel and crossed nicols.

Please cite this article as: F. Mastroianni, E. Braschi and M. Casalini et al., Data on unveiling the occurrence of transient, multi-contaminated mafic magmas inside a rhyolitic reservoir feeding an explosive eruption (Nisyros, Greece), Data in Brief, https://doi.org/10.1016/j.dib.2022.108077

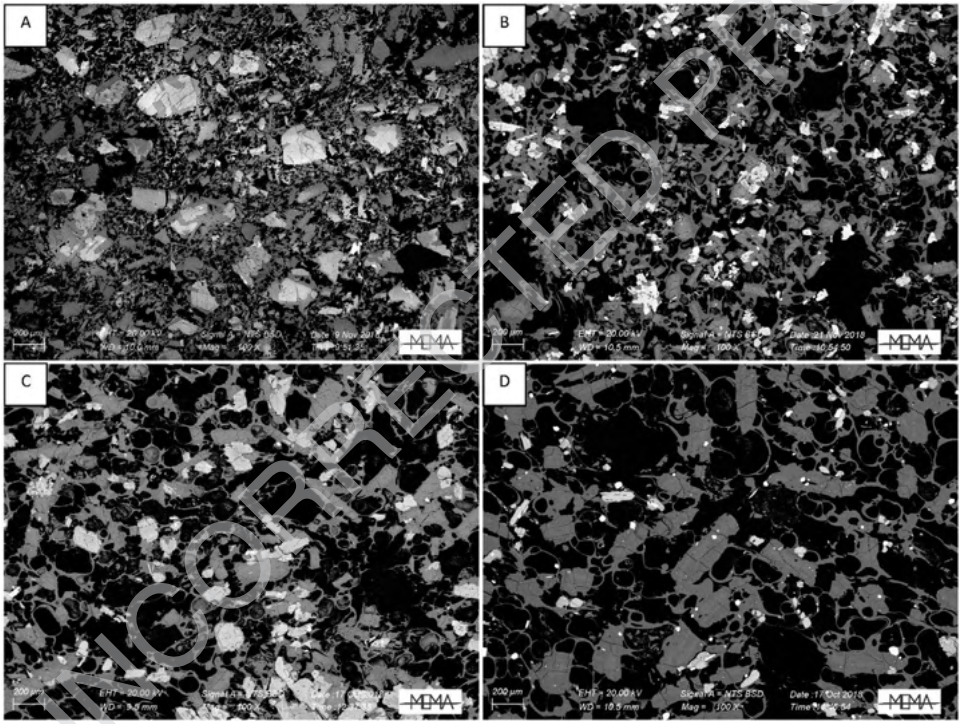

Fig. 18. BSE images of Type-B CRCs from the fallout deposit obtained by SEM observation. A: NIS357; B: NIS 368b; C: NIS364; D: NIS318.

Please cite this article as: F. Mastroianni, E. Braschi and M. Casalini et al., Data on unveiling the occurrence of transient, multi-contaminated mafic magmas inside a rhyolitic reservoir feeding an explosive eruption (Nisyros, Greece), Data in Brief, https://doi.org/10.1016/j.dib.2022.108077

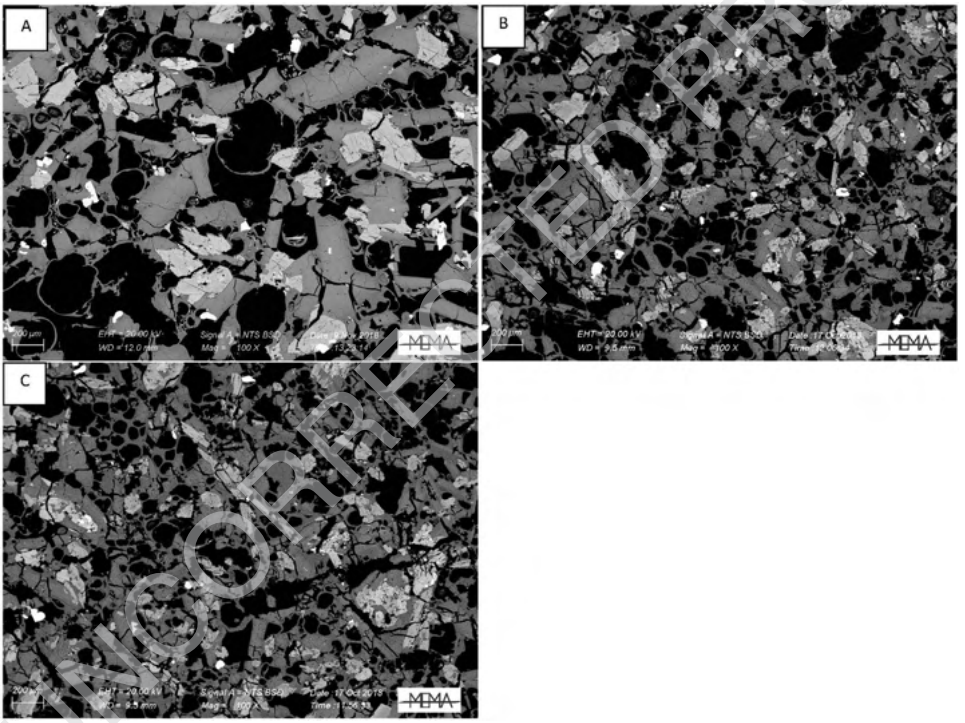

Fig. 19. BSE images of Type-B CRCs from lag-breccia deposit obtained by SEM observation. A: NIS424; B and C: NIS 430.

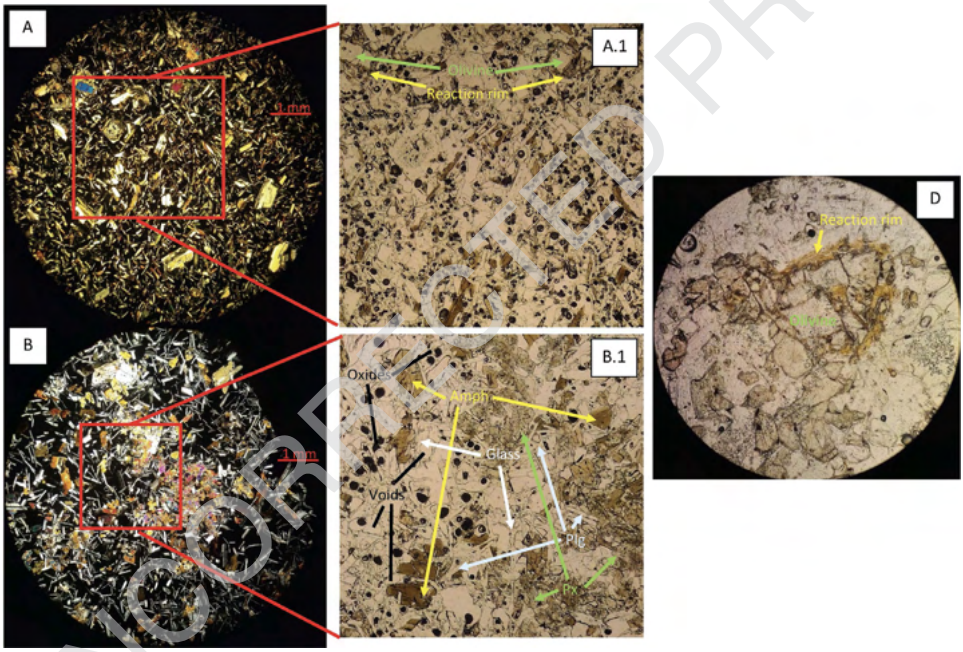

Fig. 20. Thin section microphotograph of Type-C CRCs. A: NIS422, parallel nicols detail of diktytaxitic texture and olivine with reaction rim (A.1); B: NIS421, parallel nicols detail of diktytaxitic texture and crystal cloths (B.1). D: detail of olivine with reaction rim.

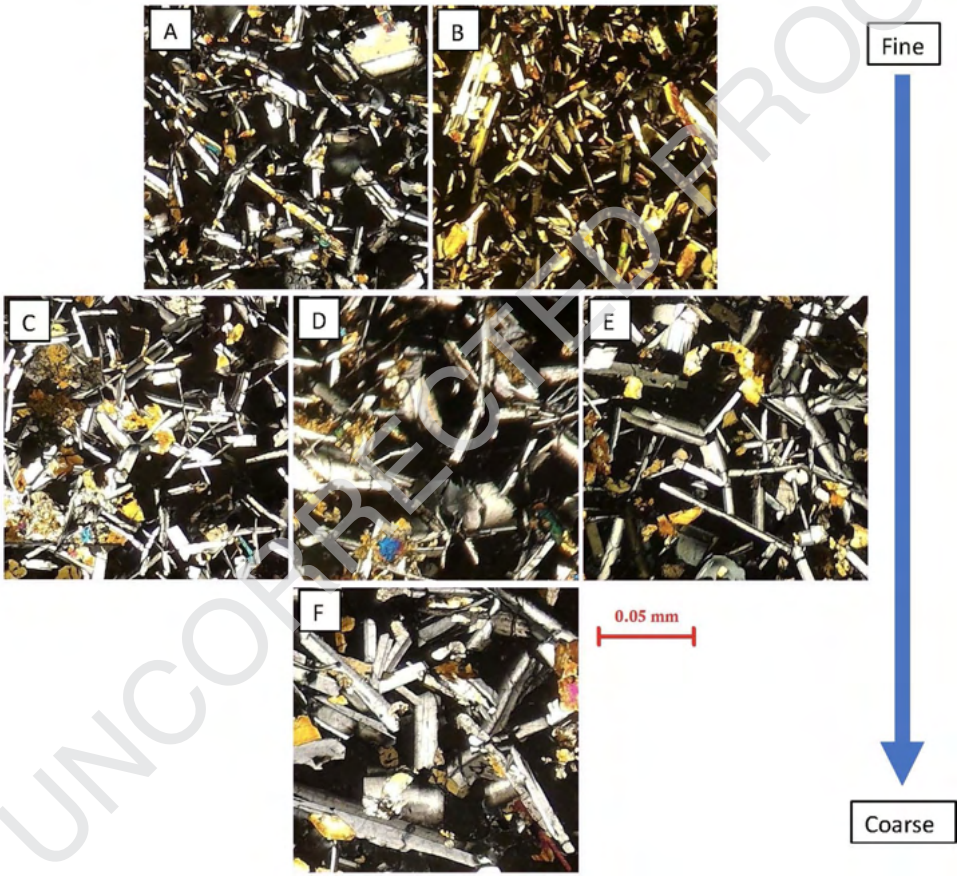

Fig. 21. Examples of the grain size variations within the Type-C samples. From the top: A, NIS421, B, NIS422; middle: C, NIS426, D, NIS427, E, NIS313; bottom: F, NIS312.

Please cite this article as: F. Mastroianni, E. Braschi and M. Casalini et al., Data on unveiling the occurrence of transient, multi-contaminated mafic magmas inside a rhyolitic reservoir feeding an explosive eruption (Nisyros, Greece), Data in Brief, https://doi.org/10.1016/j.dib.2022.108077

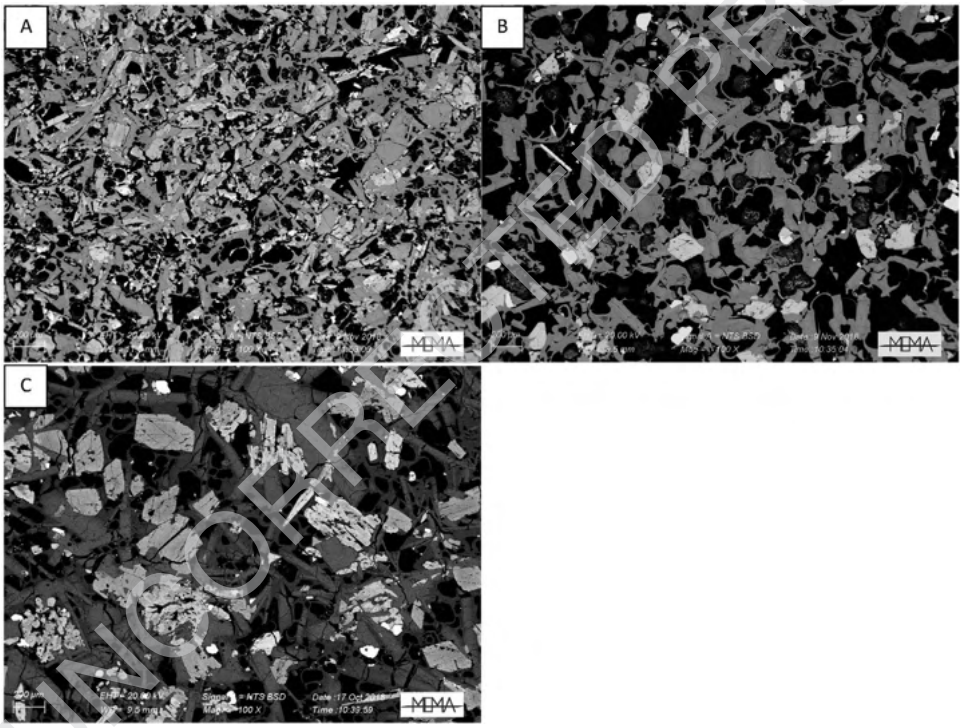

Fig. 22. BSE images of Type-C CRC samples obtained by SEM observation. A: NIS379b; B: NIS422; C: NIS428.

Please cite this article as: F. Mastroianni, E. Braschi and M. Casalini et al., Data on unveiling the occurrence of transient, multi-contaminated mafic magmas inside a rhyolitic reservoir feeding an explosive eruption (Nisyros, Greece), Data in Brief, https://doi.org/10.1016/j.dib.2022.108077

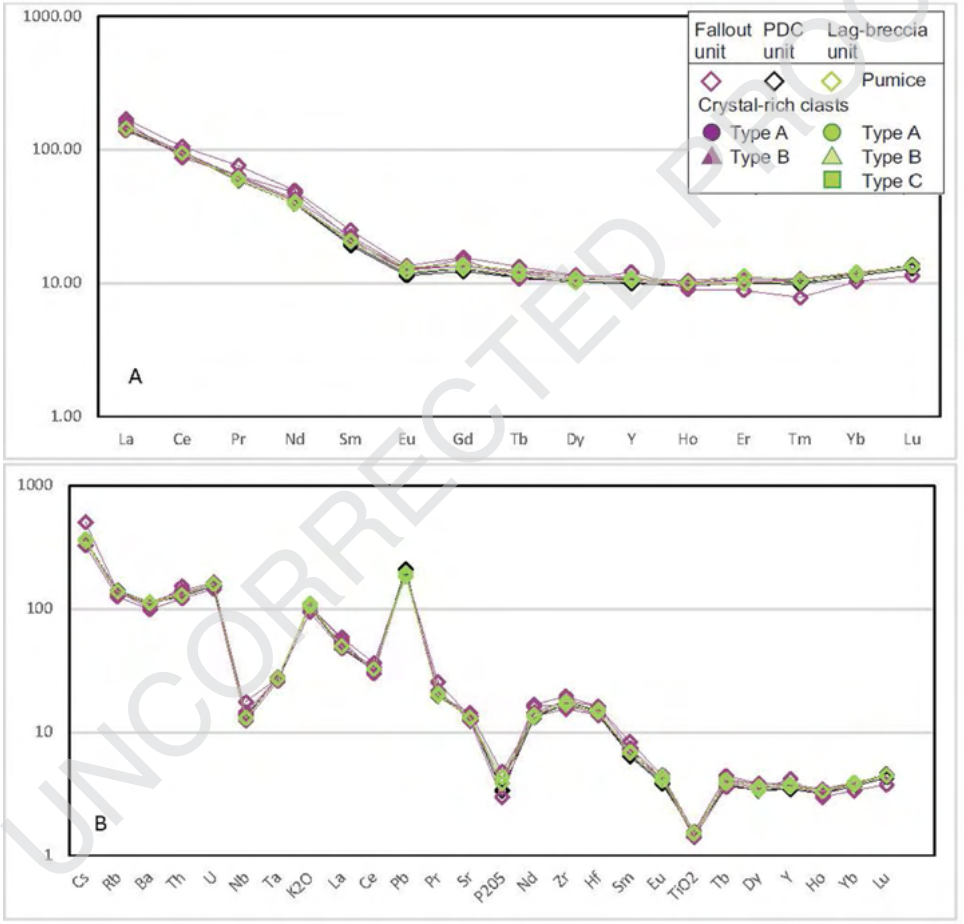

Fig. 23. REE (A) and incompatible element (B) patterns of pumice samples.

Please cite this article as: F. Mastroianni, E. Braschi and M. Casalini et al., Data on unveiling the occurrence of transient, multi-contaminated mafic magmas inside a rhyolitic reservoir feeding an explosive eruption (Nisyros, Greece), Data in Brief, https://doi.org/10.1016/j.dib.2022.108077

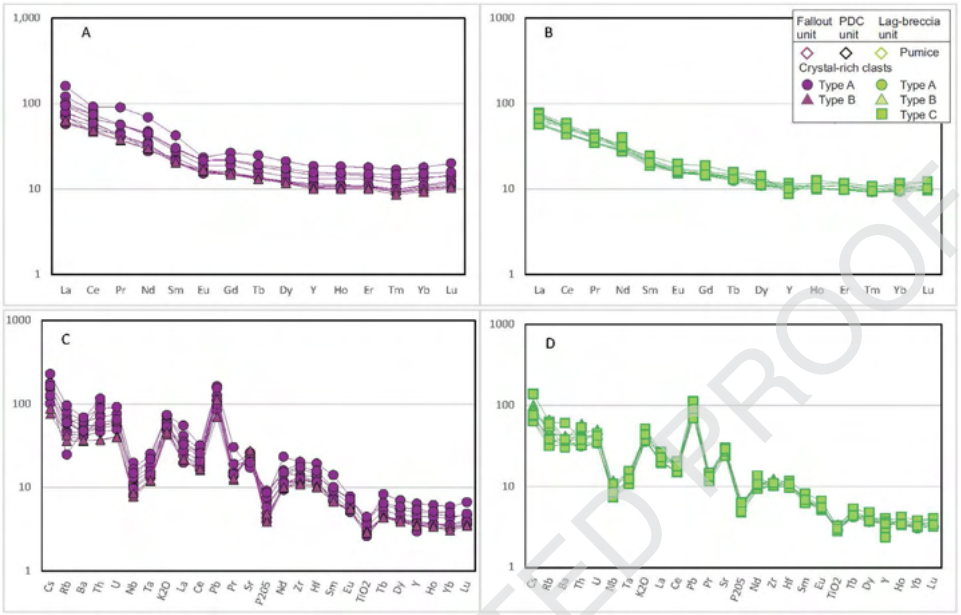

Fig. 24. REE (A and B) and incompatible element (C and D) patterns of CRC; A and C are samples from fallout and PDCs deposits, B and D are samples from lag-breccia deposits.

1.4. Mineral chemistry

In situ investigation of crystal chemistry was also performed on 10 selected samples of pumices and CRCs to explore the minerals and glass compositional variability. The following tables (Tables 3–7) report a representative selection of the mineral chemistry composition for plagioclases, pyroxenes, amphiboles and oxides, as well as the composition of glasses.

Please cite this article as: F. Mastroianni, E. Braschi and M. Casalini et al., Data on unveiling the occurrence of transient, multi-contaminated mafic magmas inside a rhyolitic reservoir feeding an explosive eruption (Nisyros, Greece), Data in Brief, https://doi.org/10.1016/j.dib.2022.108077

Table 3
Representative major and minor element composition of glasses on selected samples from the Upper Pumice deposit (Nisyros, Greece). *Footnotes*: The composition of glassy groundmasses was obtained with a Jeol JXA 8600 superprobe at the CNR-IGG in Florence. bdl= below detection limit.

Outcrop	1	1	1	1	1	1	1	1
Depositional unit	Fallout	Fallout	Fallout	Fallout	Fallout	Fallout	Fallout	Fallout
Lithology	Pumice	Pumice	Pumice	Crystal-rich Clast	Crystal-rich Clast	Crystal-rich Clast	Crystal-rich Clast	Crystal-rich Clast
Texture	Porphyritic	Porphyritic	Porphyritic	Type-A	Type-A	Type-A	Type-A	Type-A
Sample	NIS317	NIS317	NIS317	NIS317	NIS317	NIS317	NIS317	NIS317
Oxides wt%								
SiO_2	74.41	75.42	74.55	75.43	73.83	73.56	74.39	74.15
TiO_2	0.30	0.33	0.23	0.29	0.21	0.18	0.30	0.25
Al_2O_3	11.92	11.99	12.04	12.06	11.78	11.88	11.72	11.63
Cr_2O_3	0.02	0.04	bdl	bdl	0.13	bdl	0.02	bdl
FeO	1.27	1.26	1.18	1.67	1.67	1.61	1.67	1.59
MnO	bdl	0.13	0.14	bdl	0.01	0.07	0.08	0.04
MgO	0.16	0.14	0.16	0.18	0.12	0.21	0.20	0.20
CaO	0.91	0.94	0.98	1.02	1.00	1.09	1.07	0.99
Na_2O	2.82	2.56	2.47	3.12	2.91	3.18	3.02	3.02
K_2O	4.45	4.40	4.32	4.19	4.15	4.01	4.34	4.18
P_2O_5	0.06	bdl	0.06	0.06	bdl	0.05	bdl	0.04
Cl	0.18	0.17	0.28	0.40	0.32	0.28	0.32	0.35
Sum	96.50	97.38	96.41	98.42	96.13	96.11	97.14	96.43
Outcrop	1	1	1	1	1	1	1	1
Depositional unit	Fallout	Fallout	Fallout	Fallout	Fallout	Fallout	Fallout	Fallout
Lithology	Crystal-rich Clast	Crystal-rich Clast	Crystal-rich Clast	Crystal-rich Clast	Crystal-rich Clast	Crystal-rich Clast	Crystal-rich Clast	Crystal-rich Clast
Texture	Type-A	Type-A	Type-A	Type-A	Type-B	Type-B	Type-B	Type-B
Sample	NIS357	NIS357	NIS357	NIS357	NIS318	NIS318	NIS318	NIS318
Oxides wt%								
SiO_2	75.42	74.49	75.52	74.77	74.37	75.04	74.96	74.25
TiO_2	0.31	0.33	0.50	0.37	0.22	0.18	0.25	0.21
Al_2O_3	11.75	11.66	11.31	11.43	11.92	11.98	12.02	12.19
Cr_2O_3	0.03	0.05	0.01	0.01	bdl	0.01	bdl	0.05
FeO	1.60	1.28	1.32	1.54	1.33	1.62	1.21	1.29
MnO	bdl	bdl	0.04	0.06	0.06	0.03	0.06	0.03
MgO	0.14	0.21	0.20	0.23	0.14	0.17	0.14	0.17
CaO	1.02	1.13	1.01	0.91	0.92	0.95	0.85	0.88
Na_2O	3.14	3.35	3.27	2.97	2.78	2.47	2.98	2.92
K_2O	3.87	3.92	3.82	3.84	4.46	4.04	4.42	4.53

(*continued on next page*)

Table 3 (*continued*)

Outcrop	1	1	1	1	1	1	1	1
Depositional unit	Fallout	Fallout	Fallout	Fallout	Fallout	Fallout	Fallout	Fallout
Lithology	Pumice	Pumice	Pumice	Crystal-rich Clast	Crystal-rich Clast	Crystal-rich Clast	Crystal-rich Clast	Crystal-rich Clast
Texture	Porphyritic	Porphyritic	Porphyritic	Type-A	Type-A	Type-A	Type-A	Type-A
P_2O_5	bdl	bdl	0.01	bdl	0.08	bdl	0.04	0.10
Cl	0.27	0.25	0.25	0.26	0.17	0.22	0.19	0.26
Sum	97.56	96.66	97.27	96.36	96.45	96.73	97.11	96.91
Outcrop	1	5	5	5	5	5	5	8
Depositional unit	Fallout	Fallout	Fallout	Fallout	Fallout	Fallout	Fallout	Lag-breccia
Lithology	Crystal-rich Clast	Pumice	Pumice	Pumice	Pumice	Pumice	Crystal-rich Clast	Crystal-rich Clast
Texture	Type-B	Porphyritic	Porphyritic	Porphyritic	Porphyritic	Porphyritic	Type-B	Type-A
Sample	NIS318	NIS315	NIS315	NIS315	NIS315	NIS315	NIS316e	NIS420
Oxides wt%								
SiO_2	73.43	74.54	74.47	76.10	73.30	74.03	74.01	75.74
TiO_2	0.24	0.19	0.20	0.23	0.21	0.18	0.20	0.30
Al_2O_3	11.87	12.19	11.84	12.36	12.46	12.50	12.54	11.67
Cr_2O_3	0.05	bdl	bdl	bdl	0.04	bdl	0.05	0.02
FeO	1.45	1.32	1.09	1.21	1.28	1.29	1.24	1.30
MnO	0.04	0.09	bdl	0.03	0.04	0.06	0.02	0.03
MgO	0.13	0.15	0.21	0.17	0.16	0.19	0.18	0.11
CaO	0.87	0.87	0.89	0.98	1.01	0.94	0.88	0.76
Na_2O	2.96	2.75	2.81	2.71	2.28	2.37	2.33	3.30
K_2O	4.38	4.24	4.31	4.33	4.46	4.16	4.16	4.26
P_2O_5	0.02	bdl	0.07	bdl	0.03	bdl	bdl	0.05
Cl	0.21	0.18	0.21	0.20	0.21	0.17	0.27	0.34
Sum	95.67	96.53	96.09	98.31	95.48	95.89	95.88	97.88
Outcrop	8	8	8	8	8	8	8	8
Depositional unit	Lag-breccia	Lag-breccia	Lag-breccia	Lag-breccia	Lag-breccia	Lag-breccia	Lag-breccia	Lag-breccia
Lithology	Crystal-rich Clast	Crystal-rich Clast	Crystal-rich Clast	Crystal-rich Clast	Crystal-rich Clast	Crystal-rich Clast	Crystal-rich Clast	Crystal-rich Clast
Texture	Type-A	Type-A	Type-A	Type-A	Type-B	Type-B	Type-B	Type-B
Sample	NIS420	NIS420	NIS420	NIS420	NIS424	NIS424	NIS424	NIS424
Oxides wt%								
SiO_2	75.27	77.41	77.25	76.40	76.84	75.21	76.16	76.42
TiO_2	0.24	0.29	0.20	0.26	0.20	0.16	0.21	0.21
Al_2O_3	11.74	11.92	11.99	11.60	12.37	12.10	12.18	11.91

(*continued on next page*)

Table 3 (*continued*)

Outcrop	1	1	1	1	1	1	1	1
Depositional unit	Fallout	Fallout	Fallout	Fallout	Fallout	Fallout	Fallout	Fallout
Lithology	Pumice	Pumice	Pumice	Crystal-rich Clast	Crystal-rich Clast	Crystal-rich Clast	Crystal-rich Clast	Crystal-rich Clast
Texture	Porphyritic	Porphyritic	Porphyritic	Type-A	Type-A	Type-A	Type-A	Type-A
Cr_2O_3	bdl	bdl	0.04	bdl	bdl	0.04	0.05	bdl
FeO	1.18	1.03	0.50	0.94	0.90	0.97	1.25	1.10
MnO	bdl	bdl	bdl	0.03	bdl	bdl	bdl	bdl
MgO	0.20	0.13	0.07	0.11	0.03	0.14	0.13	0.13
CaO	0.83	0.84	0.55	0.83	0.70	0.78	0.71	0.67
Na_2O	2.81	3.35	2.81	2.97	2.74	3.18	3.25	3.11
K_2O	4.55	4.37	5.27	4.47	4.75	4.51	4.76	4.79
P_2O_5	bdl	0.04	bdl	bdl	bdl	bdl	0.05	bdl
Cl	0.36	0.23	0.09	0.21	bdl	0.29	0.29	bdl
Sum	97.18	99.60	98.76	97.82	98.54	97.37	99.03	98.33
Outcrop	8	8	8	8	8	8	8	8
Depositional unit	Lag-breccia	Lag-breccia	Lag-breccia	Lag-breccia	Lag-breccia	Lag-breccia	Lag-breccia	Lag-breccia
Lithology	Crystal-rich Clast	Crystal-rich Clast	Crystal-rich Clast	Crystal-rich Clast	Crystal-rich Clast	Crystal-rich Clast	Crystal-rich Clast	Crystal-rich Clast
Texture	Type-B	Type-B	Type-B	Type-B	Type-B	Type-C	Type-C	Type-C
Sample	NIS424	NIS430	NIS430	NIS430	NIS430	NIS428	NIS428	NIS428
Oxides wt%								
SiO_2	74.90	75.70	75.95	75.51	75.11	73.58	76.22	75.72
TiO_2	0.16	0.24	0.26	0.28	0.31	0.20	0.23	0.24
Al_2O_3	12.14	12.17	11.96	11.91	11.93	12.48	12.54	12.75
Cr_2O_3	bdl	0.03	bdl	bdl	0.01	bdl	0.08	bdl
FeO	1.08	1.12	0.92	1.19	1.28	1.46	1.47	1.44
MnO	bdl	bdl	bdl	bdl	0.06	bdl	0.05	bdl
MgO	0.13	0.12	0.06	0.13	0.12	0.21	0.19	0.20
CaO	0.73	0.78	0.80	0.72	0.84	1.01	0.82	0.95

(*continued on next page*)

Please cite this article as: F. Mastroianni, E. Braschi and M. Casalini et al., Data on unveiling the occurrence of transient, multi-contaminated mafic magmas inside a rhyolitic reservoir feeding an explosive eruption (Nisyros, Greece), Data in Brief, https://doi.org/10.1016/j.dib.2022.108077

Table 3 (*continued*)

Outcrop	1	1	1	1	1	1	1	1
Depositional unit	Fallout	Fallout	Fallout	Fallout	Fallout	Fallout	Fallout	Fallout
Lithology	Pumice	Pumice	Pumice	Crystal-rich Clast	Crystal-rich Clast	Crystal-rich Clast	Crystal-rich Clast	Crystal-rich Clast
Texture	Porphyritic	Porphyritic	Porphyritic	Type-A	Type-A	Type-A	Type-A	Type-A
Na_2O	2.71	2.84	3.11	3.08	2.94	3.30	3.10	2.73
K_2O	4.68	4.35	4.56	4.35	4.49	4.35	4.23	4.19
P_2O_5	0.05	0.05	bdl	bdl	bdl	0.07	bdl	0.03
Cl	0.24	0.39	0.37	0.32	0.22	0.25	0.30	0.22
Sum	96.81	97.79	97.99	97.48	97.30	96.91	99.22	98.48
Outcrop	8	8						
Depositional unit	Lag-breccia	Lag-breccia						
Lithology	Crystal-rich Clast	Crystal-rich Clast						
Texture	Type-C	Type-C						
Sample	NIS428	NIS428						
Oxides wt%								
SiO_2	74.47	74.65						
TiO_2	0.25	0.25						
Al_2O_3	12.10	12.48						
Cr_2O_3	bdl	bdl						
FeO	1.33	1.04						
MnO	0.04	0.01						
MgO	0.21	0.15						
CaO	0.91	1.06						
Na_2O	2.83	3.37						
K_2O	4.50	4.44						
P_2O_5	bdl	0.06						
Cl	0.27	0.24						
Sum	96.91	97.76						

The composition of glassy groundmasses were obtained with a Jeol JXA 8600 superprobe at the CNR-IGG in Florence. bdl= below detection limit

Please cite this article as: F. Mastroianni, E. Braschi and M. Casalini et al., Data on unveiling the occurrence of transient, multi-contaminated mafic magmas inside a rhyolitic reservoir feeding an explosive eruption (Nisyros, Greece), Data in Brief, https://doi.org/10.1016/j.dib.2022.108077

Table 4
Representative plagioclase composition (wt.%) on selected samples from the Upper Pumice deposit (Nisyros, Greece). Plagioclase crystals analysed in the pumice samples are generally more albitic (ca. 30 % An) than those in CRCs (>60 % An). *Footnotes*: gdm=crystal size <0.5 mm. Ab= Albite, An= Anorthite; Or= Orthoclase.

Outcrop	1	1	1	1	1	1	1	1	1
Depositional unit	Fallout	Fallout	Fallout	Fallout	Fallout	Fallout	Fallout	Fallout	Fallout
Lithology	Banded Pumice	Banded Pumice	Banded Pumice	Banded Pumice	Crystal-rich portion	Crystal-rich portion	Crystal-rich portion	Crystal-rich portion	Crystal-rich clast
Texture	Porphyritic	Porphyritic	Porphyritic	Porphyritic	Type-A	Type-A	Type-A	Type-A	Type-A
Sample	NIS317	NIS317	NIS317	NIS317	NIS317	NIS317	NIS317	NIS317	NIS357
Zone	core	rim	core	rim	core	rim	gdm	gdm	core
SiO_2	51.81	62.31	60.96	61.31	50.96	59.41	52.34	59.08	50.02
TiO_2	0.05	0.10	bdl	bdl	0.04	0.01	bdl	bdl	0.03
Al_2O_3	30.19	24.16	24.31	24.47	30.80	24.86	29.32	25.09	31.38
Fe_2O_3	0.59	0.30	0.33	0.39	0.50	0.40	0.42	0.39	0.56
MgO	0.08	bdl	0.04	bdl	0.08	0.04	0.03	bdl	0.06
CaO	13.89	5.63	6.51	6.44	13.75	7.13	12.36	7.86	14.38
Na_2O	3.45	7.25	6.82	6.90	3.89	7.10	4.38	6.96	3.57
K_2O	0.17	0.91	0.75	0.73	0.09	0.53	0.16	0.57	0.13
Sum	100.24	100.66	99.71	100.24	100.10	99.46	99.01	99.95	100.12
FeO	0.530	0.269	0.296	0.354	0.449	0.359	0.380	0.349	0.507
Si	2.352	2.747	2.719	2.719	2.321	2.668	2.398	2.648	2.284
Al	1.616	1.255	1.278	1.279	1.653	1.316	1.583	1.325	1.688
Ti	0.002	0.003	0.000	0.000	0.001	0.000	0.000	0.000	0.001
Fe3+	0.020	0.010	0.011	0.013	0.017	0.013	0.015	0.013	0.019
Mg	0.006	0.000	0.003	0.000	0.005	0.002	0.002	0.000	0.004
Ca	0.676	0.266	0.311	0.306	0.671	0.343	0.607	0.377	0.703
Na	0.304	0.620	0.590	0.593	0.344	0.618	0.389	0.605	0.316
K	0.010	0.051	0.043	0.042	0.005	0.030	0.009	0.032	0.008
Ab	30.71	66.14	62.52	63.08	33.70	62.33	38.71	59.62	30.77
An	68.28	28.39	32.94	32.51	65.81	34.61	60.36	37.18	68.48
Or	1.01	5.48	4.53	4.41	0.49	3.06	0.93	3.20	0.75
Outcrop	1	1	1	1	1	1	1	5	5
Depositional unit	Fallout	Fallout	Fallout	Fallout	Fallout	Fallout	Fallout	Fallout	Fallout
Lithology	Crystal-rich clast	Crystal-rich clast	Crystal-rich clast	Crystal-rich clast	Crystal-rich clast	Crystal-rich clast	Crystal-rich clast	Pumice	Pumice
Texture	Type-C	Type-C	Type-C	Type-A	Type-A	Type-A	Type-A	Porphyritic	Porphyritic
Sample	NIS368c	NIS368c	NIS368c	NIS369a	NIS369a	NIS369a	NIS369a	NIS315	NIS315
Zone	core	rim	core	Core	Core	Core	Rim	core	rim
SiO_2	49.28	57.14	46.70	48.81	46.26	48.30	59.50	61.52	60.33
TiO_2	bdl	0.04	0.02	bdl	0.07	0.02	bdl	bdl	bdl
Al_2O_3	32.40	28.21	34.66	31.58	32.59	32.85	25.59	24.36	24.30
Fe_2O_3	0.60	0.39	0.42	0.60	0.45	0.47	0.53	0.24	0.41
MgO	0.09	0.07	bdl	0.14	0.19	0.10	0.08	0.02	bdl
CaO	15.49	9.55	17.55	15.50	17.47	15.89	7.74	6.02	6.89
Na_2O	2.29	4.93	1.33	3.20	1.73	2.52	6.12	7.33	6.90

(*continued on next page*)

Table 4 (*continued*)

Outcrop	1	1	1	1	1	1	1	1	1
Depositional unit	Fallout	Fallout	Fallout	Fallout	Fallout	Fallout	Fallout	Fallout	Fallout
Lithology	Banded Pumice	Banded Pumice	Banded Pumice	Banded Pumice	Crystal-rich portion	Crystal-rich portion	Crystal-rich portion	Crystal-rich portion	Crystal-rich clast
Texture	Porphyritic	Porphyritic	Porphyritic	Porphyritic	Type-A	Type-A	Type-A	Type-A	Type-A
K_2O	0.15	0.42	bdl	0.11	0.17	bdl	0.56	0.72	0.66
Sum	100.30	100.75	100.67	99.94	98.93	100.14	100.12	100.21	99.49
FeO	0.538	0.355	0.374	0.544	0.406	0.426	0.475	0.220	0.370
Si	2.246	2.539	2.132	2.240	2.157	2.210	2.648	2.725	2.702
Al	1.740	1.478	1.865	1.708	1.791	1.771	1.342	1.272	1.283
Ti	0.000	0.001	0.001	0.000	0.002	0.001	0.000	0.000	0.000
Fe3+	0.020	0.013	0.014	0.021	0.016	0.016	0.018	0.008	0.014
Mg	0.006	0.005	0.000	0.009	0.013	0.007	0.005	0.001	0.000
Ca	0.756	0.454	0.858	0.762	0.873	0.779	0.369	0.286	0.331
Na	0.202	0.425	0.118	0.285	0.156	0.223	0.528	0.630	0.599
K	0.009	0.024	0.000	0.007	0.010	0.000	0.032	0.041	0.038
Ab	20.92	47.03	12.05	26.9	15.0	22.3	56.8	65.80	61.91
An	78.17	50.34	87.95	72.1	84.0	77.7	39.7	29.86	34.16
Or	0.91	2.64	0.00	0.62	0.95	0.00	3.41	4.25	3.90
Outcrop	5	5	5	5	8	8	8	8	8
Depositional unit	Fallout	Fallout	Fallout	Fallout	Lag-breccia	Lag-breccia	Lag-breccia	Lag-breccia	Lag-breccia
Lithology	Pumice	Pumice	Crystal-rich clast	Crystal-rich clast	Crystal-rich clast	Crystal-rich clast	Crystal-rich clast	Crystal-rich clast	Crystal-rich clast
Texture	Porphyritic	Porphyritic	Type-B	Type-B	Type-A	Type-A	Type-A	Type-B	Type-B
Sample	NIS315	NIS315	NIS316e	NIS316e	NIS420	NIS420	NIS420	NIS424	NIS424
Zone	core	rim	core	rim	core	core	gdm	core	core
SiO_2	61.60	60.66	56.52	57.67	49.79	51.00	52.40	47.32	59.45
TiO_2	bdl	bdl	bdl	bdl	0.07	0.01	bdl	bsl	0.09
Al_2O_3	24.12	24.59	27.74	27.07	30.62	30.53	29.96	33.42	25.12
Fe_2O_3	0.12	0.31	0.44	0.27	0.60	0.64	0.50	0.65	0.54
MgO	bdl	bdl	bdl	0.02	0.02	0.14	0.05	0.16	bdl
CaO	5.61	6.23	9.43	8.64	14.09	13.95	13.04	17.27	7.58
Na_2O	7.61	7.34	6.07	5.96	3.35	3.65	4.79	1.68	6.12
K_2O	0.82	0.69	0.34	0.44	0.08	0.11	0.12	0.07	0.55
Sum	99.88	99.82	100.54	100.07	98.64	100.02	100.85	100.57	99.44
FeO	0.110	0.280	0.400	0.240	0.544	0.580	0.446	0.583	0.484
Si	2.739	2.703	2.527	2.580	2.303	2.325	2.367	2.165	2.665
Al	1.264	1.291	1.462	1.427	1.670	1.641	1.595	1.802	1.327

(*continued on next page*)

Please cite this article as: F. Mastroianni, E. Braschi and M. Casalini et al., Data on unveiling the occurrence of transient, multi-contaminated mafic magmas inside a rhyolitic reservoir feeding an explosive eruption (Nisyros, Greece), Data in Brief, https://doi.org/10.1016/j.dib.2022.108077

Table 4 (*continued*)

Outcrop	1	1	1	1	1	1	1	1	1
Depositional unit	Fallout	Fallout	Fallout	Fallout	Fallout	Fallout	Fallout	Fallout	Fallout
Lithology	Banded Pumice	Banded Pumice	Banded Pumice	Banded Pumice	Crystal-rich portion	Crystal-rich portion	Crystal-rich portion	Crystal-rich portion	Crystal-rich clast
Texture	Porphyritic	Porphyritic	Porphyritic	Porphyritic	Type-A	Type-A	Type-A	Type-A	Type-A
Ti	0.000	0.000	0.000	0.000	0.002	0.000	0.000	0.000	0.003
Fe3+	0.004	0.010	0.015	0.009	0.021	0.022	0.017	0.022	0.018
Mg	0.000	0.000	0.000	0.001	0.002	0.009	0.003	0.011	0.000
Ca	0.267	0.297	0.452	0.414	0.698	0.682	0.631	0.847	0.364
Na	0.656	0.634	0.526	0.517	0.301	0.322	0.419	0.149	0.532
K	0.047	0.039	0.019	0.025	0.005	0.006	0.007	0.004	0.031
Ab	67.51	65.13	52.72	54.04	29.95	31.91	39.66	14.94	57.34
An	27.50	30.55	45.26	43.29	69.57	67.48	59.68	84.67	39.27
Or	4.79	4.03	1.94	2.63	0.48	0.61	0.66	0.39	3.39
Outcrop	8	8	8	8	8	8	8	8	8
Depositional unit	Lag-breccia	Lag-breccia	Lag-breccia	Lag-breccia	Lag-breccia	Lag-breccia	Lag-breccia	Lag-breccia	Lag-breccia
Lithology	Crystal-rich clast	Crystal-rich clast	Crystal-rich clast	Crystal-rich clast	Crystal-rich clast	Crystal-rich clast	Crystal-rich clast	Crystal-rich clast	Crystal-rich clast
Texture	Type-B	Type-B	Type-C	Type-C	Type-C	Type-B	Type-B	Type-B	Type-B
Sample	NIS424	NIS424	NIS428	NIS428	NIS428	NIS430	NIS430	NIS430	NIS430
Zone	core	core	core	rim	core	core	core	rim	core
SiO_2	51.46	49.35	46.92	56.42	48.71	52.03	46.30	46.85	57.63
TiO_2	0.11	0.06	0.05	bdl	bdl	bdl	bdl	0.10	bdl
Al_2O_3	29.70	31.79	32.97	27.06	31.05	30.48	33.67	33.14	25.73
Fe_2O_3	0.65	0.49	0.58	0.54	0.88	0.59	0.44	0.61	0.42
MgO	0.07	0.11	0.09	0.03	0.02	0.06	0.01	0.06	0.05
CaO	13.18	15.72	17.23	9.49	15.63	13.30	17.17	17.12	9.17
Na_2O	4.05	2.75	1.81	5.91	2.73	4.20	1.63	1.82	5.50
K_2O	0.16	0.05	0.08	0.44	0.12	0.15	0.04	0.03	0.69
Sum	99.37	100.32	99.74	99.90	99.15	100.80	99.26	99.73	99.18
FeO	0.589	0.437	0.523	0.484	0.795	0.529	0.396	0.549	0.382
Si	2.358	2.253	2.166	2.543	2.255	2.350	2.145	2.162	2.606
Al	1.604	1.710	1.794	1.437	1.694	1.623	1.839	1.803	1.371
Ti	0.004	0.002	0.002	0.000	0.000	0.000	0.000	0.003	0.000
Fe3+	0.023	0.017	0.020	0.018	0.031	0.020	0.015	0.021	0.014
Mg	0.005	0.008	0.006	0.002	0.002	0.004	0.001	0.004	0.003
Ca	0.647	0.769	0.853	0.458	0.775	0.643	0.852	0.846	0.444
Na	0.360	0.244	0.162	0.516	0.245	0.368	0.147	0.163	0.482
K	0.009	0.003	0.005	0.026	0.007	0.009	0.002	0.002	0.040
Ab	35.41	23.98	15.91	51.63	23.85	36.05	14.66	16.13	49.89
An	63.70	75.71	83.65	45.81	75.43	63.11	85.10	83.66	45.98
Or	0.89	0.31	0.44	2.55	0.71	0.84	0.24	0.20	4.13

Footnotes: gdm=crystal size <0.5 mm. Ab= Albite, An= Anorthite; Or= Orthoclase.

Please cite this article as: F. Mastroianni, E. Braschi and M. Casalini et al., Data on unveiling the occurrence of transient, multi-contaminated mafic magmas inside a rhyolitic reservoir feeding an explosive eruption (Nisyros, Greece), Data in Brief, https://doi.org/10.1016/j.dib.2022.108077

Table 5
Representative pyroxene composition (wt.%) on selected samples from the Upper Pumice deposit (Nisyros, Greece). The pyroxenes are mostly orthopyroxenes; clinopyroxenes are less common and are generally found as microcrystals or in aggregates. *Footnotes*: cpx: clinopyroxene; opx: orthopyroxene; bdl = below detection limit; En= Enstatite; Fe= Ferrosilite; Wo= Wollastonite; Mg#: molecular Mg/(Mg+Fe+Mn).

Outcrop	1	1	1	1	1	1	1	1	1	1	1	1	1	1	1	5	5
Depositional unit	Fallout	Fallout	Fallout	Fallout	Fallout	Fallout	Fallout	Fallout	Fallout	Fallout	Fallout	Fallout	Fallout	Fallout	Fallout	Fallout	Fallout
Lithology	Pumice	CRC	CRC	CRC	CRC	CRC	CRC	CRC	CRC	CRC	CRC	CRC	CRC	CRC	CRC	Pumice	Pumice
Texture	Porphyritic	Type-A	Type-A	Type-A	Type-A	Type-A	Type-A	Type-A	Type-A	Type-A	Type-B	Type-B	Type-C	Type-C	Type-C	Porphyritic	Porphyritic
Sample	NIS317	NIS317	NIS317	NIS357	NIS357	NIS368d	NIS368d	NIS369a	NIS369a	NIS369a	NIS318	NIS318	NIS368c	NIS368c	NIS368c	NIS315	NIS315
Phase	opx	opx	opx	opx	opx	opx	opx	opx	opx	cpx	opx	cpx	opx	opx	opx	opx	opx
Zone	core	core	core	core	rim	core	rim	core	core	core	core	core	core	rim	core	core	rim
SiO_2	52.51	51.02	50.45	55.68	52.20	53.50	51.59	51.42	51.78	51.73	51.12	52.44	53.00	54.25	53.05	52.72	52.99
TiO_2	0.10	0.23	0.31	0.22	0.25	0.17	0.14	0.09	0.17	0.66	0.21	0.28	0.21	0.09	0.17	0.14	0.13
Al_2O_3	0.32	0.75	2.05	1.85	1.83	1.74	0.54	0.29	0.57	1.93	0.93	1.05	0.80	1.80	0.60	0.50	0.32
FeO	25.07	27.20	27.65	11.57	24.32	15.32	25.44	27.63	23.46	12.09	25.95	11.20	19.32	13.11	20.49	23.64	23.81
MnO	1.28	0.93	0.73	0.28	0.66	0.36	0.70	0.79	0.54	0.37	1.19	0.47	0.54	0.34	0.68	1.25	1.16
MgO	20.08	18.36	18.33	28.83	20.28	26.91	20.28	19.00	21.23	13.48	19.41	13.40	24.49	28.84	23.61	20.51	21.02
CaO	1.16	1.21	0.91	1.76	1.16	1.31	0.97	1.26	1.84	19.46	0.92	21.38	1.28	1.74	1.25	1.14	1.02
Na_2O	0.03	bdl	bdl	bdl	bdl	0.02	0.02	bdl	0.08	0.27	bdl	0.35	0.03	0.11	0.04	0.09	bdl
K_2O	0.06	0.02	0.02	bdl	0.02	0.02	bdl	0.08	bdl	bdl	bdl	bdl	bdl	0.05	bdl	0.02	bdl
Sum	100.60	99.72	100.45	100.19	100.70	99.37	99.68	100.56	99.67	99.98	99.73	100.56	99.69	100.33	99.88	100.01	100.45
SiO_2	52.51	51.02	50.45	55.68	52.20	53.50	51.59	51.42	51.78	51.73	51.12	52.44	53.00	54.25	53.05	52.72	52.99
TiO_2	0.10	0.23	0.31	0.22	0.25	0.17	0.14	0.09	0.17	0.66	0.21	0.28	0.21	0.09	0.17	0.14	0.13
Al_2O_3	0.32	0.75	2.05	1.85	1.83	1.74	0.54	0.29	0.57	1.93	0.93	1.05	0.80	1.80	0.60	0.50	0.32
Fe_2O_3	1.21	1.42	1.89	bdl	0.02	1.51	2.03	2.89	2.80	0.26	1.78	1.78	1.98	3.12	1.63	0.27	0.31
FeO	23.98	25.93	25.95	11.57	24.30	13.95	23.61	25.04	20.93	11.86	24.35	9.59	17.55	10.30	19.02	23.40	23.53
MnO	1.28	0.93	0.73	0.28	0.66	0.36	0.70	0.79	0.54	0.37	1.19	0.47	0.54	0.34	0.68	1.25	1.16
MgO	20.08	18.36	18.33	28.83	20.28	26.91	20.28	19.00	21.23	13.48	19.41	13.40	24.49	28.84	23.61	20.51	21.02
CaO	1.16	1.21	0.91	1.76	1.16	1.31	0.97	1.26	1.84	19.46	0.92	21.38	1.28	1.74	1.25	1.14	1.02
Na_2O	0.03	bdl	bdl	bdl	bdl	0.02	0.02	bdl	0.08	0.27	bdl	0.35	0.03	0.11	0.04	0.09	bdl
K_2O	0.06	0.02	0.02	bdl	0.02	0.02	bdl	0.08	bdl	bdl	bdl	bdl	bdl	0.05	bdl	0.02	bdl
sum	100.72	99.87	100.64	100.22	100.71	99.52	99.88	100.85	99.95	100.02	99.91	100.79	99.89	100.64	100.07	100.06	100.48
Si	1.975	1.957	1.919	1.974	1.953	1.94	1.96	1.952	1.946	1.945	1.948	1.956	1.951	1.923	1.961	1.985	1.985
Al	0.014	0.034	0.081	0.026	0.047	0.06	0.02	0.013	0.025	0.055	0.042	0.044	0.035	0.075	0.026	0.015	0.014
Ti	0.003	0.007	0.000	0.000	0.000	0.00	0.00	0.003	0.005	0.000	0.006	0.000	0.006	0.001	0.005	0.000	0.001
Fe^{3+}	0.007	0.003	0.000	0.000	0.000	0.00	0.02	0.033	0.024	0.000	0.005	0.000	0.009	0.000	0.009	0.000	0.000
Al	0.000	0.000	0.011	0.051	0.033	0.01	0.00	0.000	0.000	0.030	0.000	0.002	0.000	0.000	0.000	0.007	0.000
Ti	0.000	0.000	0.009	0.006	0.007	0.00	0.00	0.000	0.000	0.019	0.000	0.008	0.000	0.001	0.000	0.004	0.003
Fe^{3+}	0.027	0.038	0.054	0.000	0.001	0.04	0.04	0.050	0.055	0.007	0.046	0.050	0.046	0.083	0.037	0.008	0.009
Mg	1.126	1.050	1.039	1.524	1.131	1.45	1.15	1.075	1.190	0.755	1.102	0.745	1.344	1.524	1.301	1.151	1.174
Fe^{2+}	0.755	0.831	0.825	0.343	0.760	0.42	0.75	0.795	0.658	0.373	0.776	0.299	0.540	0.305	0.588	0.737	0.737
Mn	0.041	0.030	0.024	0.008	0.021	0.01	0.02	0.025	0.017	0.012	0.038	0.015	0.017	0.010	0.021	0.040	0.037
Ca	0.047	0.050	0.037	0.067	0.046	0.05	0.04	0.051	0.074	0.784	0.037	0.854	0.051	0.066	0.050	0.046	0.041

(*continued on next page*)

Please cite this article as: F. Mastroianni, E. Braschi and M. Casalini et al., Data on unveiling the occurrence of transient, multi-contaminated mafic magmas inside a rhyolitic reservoir feeding an explosive eruption (Nisyros, Greece), Data in Brief, https://doi.org/10.1016/j.dib.2022.108077

Table 5 (*continued*)

Outcrop	1	1	1	1	1	1	1	1	1	1	1	1	1	1	1	5	5
Depositional unit	Fallout	Fallout	Fallout	Fallout	Fallout	Fallout	Fallout	Fallout	Fallout	Fallout	Fallout	Fallout	Fallout	Fallout	Fallout	Fallout	Fallout
Lithology	Pumice	CRC	CRC	CRC	CRC	CRC	CRC	CRC	CRC	CRC	CRC	CRC	CRC	CRC	CRC	Pumice	Pumice
Texture	Porphyritic	Type-A	Type-A	Type-A	Type-A	Type-A	Type-A	Type-A	Type-A	Type-A	Type-A	Type-B	Type-B	Type-C	Type-C	Porphyritic	Porphyritic
Na	0.002	0.000	0.000	0.000	0.000	0.00	0.00	0.000	0.006	0.019	0.000	0.025	0.002	0.008	0.003	0.007	0.000
K	0.003	0.001	0.001	0.000	0.001	0.00	0.00	0.004	0.000	0.000	0.000	0.000	0.000	0.002	0.000	0.001	0.000
En	56.24	52.43	52.50	78.46	57.73	73.43	56.89	53.0	58.9	39.11	54.99	37.96	67.0	76.6	64.9	58.10	58.77
Fe	41.43	45.09	45.61	18.09	39.90	24.01	41.15	44.5	37.4	20.29	43.15	18.54	30.5	20.1	32.6	39.58	39.18
Wo	2.33	2.49	1.88	3.45	2.37	2.56	1.96	2.5	3.7	40.59	1.86	43.50	2.5	3.3	2.5	2.32	2.05
Mg#	0.58	0.54	0.54	0.81	0.59	0.75	0.58	0.54	0.61	0.66	0.56	0.67	0.69	0.79	0.67	0.59	0.60

Outcrop	5	5	8	8	8	8	8	8	8	8	8	8	8
Depositional unit	Fallout	Fallout	Lag-breccia	Lag-breccia	Lag-breccia	Lag-breccia	Lag-breccia	Lag-breccia	Lag-breccia	Lag-breccia	Lag-breccia	Lag-breccia	Lag-breccia
Lithology	Pumice	CRC	CRC	CRC	CRC	CRC	CRC	CRC	CRC	CRC	CRC	CRC	CRC
Texture	Porphyritic	Type-B	Type-A	Type-A	Type-A	Type-A	Type-A	Type-B	Type-B	Type-B	Type-B	Type-C	Type-C
Sample	NIS315	NIS316e	NIS420	NIS420	NIS420	NIS420	NIS420	NIS424	NIS424	NIS424	NIS430	NIS428	NIS428
Phase	cpx	opx	cpx	opx	opx	opx	opx	cpx	opx	opx	opx	opx	opx
Zone	core	core		core	rim	core	rim	core	core	core			
SiO_2	51.81	50.72	52.87	53.66	52.97	52.63	53.03	52.36	52.27	54.17	52.94	51.73	52.11
TiO_2	0.40	0.14	0.30	0.33	0.11	0.24	0.11	0.33	0.15	0.12	0.04	0.21	0.25
Al_2O_3	1.60	0.76	0.93	3.31	0.72	4.67	0.45	1.05	0.75	2.37	0.25	1.58	2.19
FeO	9.88	27.39	11.34	14.33	23.13	13.10	24.95	10.35	22.43	17.21	23.32	22.62	20.78
MnO	0.48	1.25	0.29	0.18	0.67	0.23	0.71	0.38	0.85	0.30	0.87	0.65	0.58
MgO	13.90	18.42	14.31	26.45	21.65	26.87	20.74	13.96	21.54	26.59	21.36	21.59	23.13
CaO	21.80	0.96	19.98	2.25	0.89	1.70	0.80	21.74	1.37	0.63	1.03	1.23	1.28
Na_2O	bdl	bdl	0.24	bdl	bdl	0.04	bdl	0.37	0.13	0.03	bdl	0.07	0.08
K_2O	bdl	bdl	bdl	bdl	0.02	bdl	0.01	0.03	bdl	bdl	0.01	bdl	0.04
Sum	99.87	99.64	100.26	100.52	100.16	99.48	100.82	100.57	99.49	101.42	99.83	99.68	100.45
SiO_2	51.81	50.72	52.87	53.66	52.97	52.63	53.03	52.36	52.27	54.17	52.94	51.73	52.11
TiO_2	0.40	0.14	0.30	0.33	0.11	0.24	0.11	0.33	0.15	0.12	0.04	0.21	0.25
Al_2O_3	1.60	0.76	0.93	3.31	0.72	4.67	0.45	1.05	0.75	2.37	0.25	1.58	2.19
Fe_2O_3	0.85	2.16	0.38	0.10	0.18	0.47	0.23	2.64	1.53	1.10	0.32	1.78	2.46
FeO	9.12	25.44	11.00	14.25	22.97	12.68	24.75	7.98	21.06	16.22	23.03	21.01	18.57
MnO	0.48	1.25	0.29	0.18	0.67	0.23	0.71	0.38	0.85	0.30	0.87	0.65	0.58
MgO	13.90	18.42	14.31	26.45	21.65	26.87	20.74	13.96	21.54	26.59	21.36	21.59	23.13
CaO	21.80	0.96	19.98	2.25	0.89	1.70	0.80	21.74	1.37	0.63	1.03	1.23	1.28
Na_2O	bdl	bdl	0.24	bdl	bdl	0.04	bdl	0.37	0.13	0.03	bdl	0.07	0.08
K_2O	bdl	bdl	bdl	bdl	0.02	bdl	0.01	0.03	bdl	bdl	0.01	bdl	0.04
sum	99.98	99.90	100.30	100.53	100.17	99.53	100.84	100.83	99.71	101.53	99.88	99.91	100.76
Si	1.941	1.947	1.974	1.920	1.979	1.890	1.984	1.945	1.961	1.933	1.989	1.936	1.915
Al	0.059	0.034	0.026	0.080	0.021	0.110	0.016	0.046	0.033	0.067	0.011	0.064	0.085

(*continued on next page*)

Please cite this article as: F. Mastroianni, E. Braschi and M. Casalini et al., Data on unveiling the occurrence of transient, multi-contaminated mafic magmas inside a rhyolitic reservoir feeding an explosive eruption (Nisyros, Greece), Data in Brief, https://doi.org/10.1016/j.dib.2022.108077

Table 5 (*continued*)

Outcrop	1	1	1	1	1	1	1	1	1	1	1	1	1	5	5
Depositional unit	Fallout	Fallout	Fallout	Fallout	Fallout	Fallout	Fallout	Fallout	Fallout	Fallout	Fallout	Fallout	Fallout	Fallout	Fallout
Lithology	Pumice	CRC	CRC	CRC	CRC	CRC	CRC	CRC	CRC	CRC	CRC	CRC	CRC	Pumice	Pumice
Texture	Porphyritic	Type-A	Type-A	Type-A	Type-A	Type-A	Type-A	Type-A	Type-A	Type-B	Type-B	Type-C	Type-C	Porphyritic	Porphyritic
Ti	0.000	0.004	0.000	0.000	0.000	0.000	0.000	0.009	0.004	0.000	0.000	0.000	0.000		
Fe^{3+}	0.000	0.015	0.000	0.000	0.000	0.000	0.000	0.000	0.002	0.000	0.000	0.000	0.000		
Al	0.012	0.000	0.015	0.060	0.011	0.087	0.004	0.000	0.000	0.033	0.000	0.006	0.009		
Ti	0.011	0.000	0.009	0.009	0.003	0.007	0.003	0.000	0.000	0.003	0.001	0.006	0.007		
Fe^{3+}	0.024	0.048	0.011	0.003	0.005	0.013	0.006	0.074	0.042	0.030	0.009	0.050	0.068		
Mg	0.776	1.054	0.796	1.411	1.206	1.438	1.157	0.773	1.205	1.415	1.196	1.205	1.267		
Fe^{2+}	0.286	0.817	0.344	0.426	0.718	0.381	0.774	0.248	0.661	0.484	0.723	0.658	0.571		
Mn	0.015	0.041	0.009	0.005	0.021	0.007	0.023	0.012	0.027	0.009	0.028	0.021	0.018		
Ca	0.875	0.039	0.799	0.086	0.035	0.065	0.032	0.865	0.055	0.024	0.042	0.049	0.050		
Na	0.000	0.000	0.017	0.000	0.000	0.003	0.000	0.027	0.009	0.002	0.000	0.005	0.006		
K	0.000	0.000	0.000	0.000	0.001	0.000	0.001	0.001	0.000	0.000	0.001	0.000	0.002		
En	39.28	52.35	40.65	73.05	60.74	75.53	58.06	39.20	60.52	72.12	59.87	60.76	64.18		
Fe	16.44	45.69	18.55	22.49	37.48	21.03	40.33	16.92	36.71	26.66	38.05	36.75	33.27		
Wo	44.28	1.96	40.80	4.47	1.79	3.43	1.61	43.88	2.77	1.22	2.08	2.49	2.55		
Mg#	0.71	0.53	0.69	0.76	0.62	0.78	0.59	0.70	0.62	0.73	0.61	0.62	0.66		

cpx: clinopyroxene; opx: orthopyroxene; bdl = below detection limit; En= Enstatite; Fe= Ferrosilite; Wo= Wollastonite; Mg#: molecular Mg/(Mg+Fe+Mn)

Please cite this article as: F. Mastroianni, E. Braschi and M. Casalini et al., Data on unveiling the occurrence of transient, multi-contaminated mafic magmas inside a rhyolitic reservoir feeding an explosive eruption (Nisyros, Greece), Data in Brief, https://doi.org/10.1016/j.dib.2022.108077

Table 6
Representative amphibole composition (wt.%) on selected samples from the Upper Pumice deposit (Nisyros, Greece). Amphiboles are ubiquitous in the CRC samples and rare in pumices. *Footnotes:* bdl= below detection limit; * calculated on stoichiometric basis [10].

Outcrop	1	1	1	1	1	8	8	8
Depositional unit	Fallout	Fallout	Fallout	Fallout	Fallout	Lag-breccia	Lag-breccia	Lag-breccia
Lithology	CRC	CRC	CRC	CRC	CRC	CRC	CRC	CRC
Texture	Type-A	Type-A	Type-A	Type-A	Type-A	Type-A	Type-B	Type-C
Sample	NIS357	NIS357	NIS368d	NIS369a	NIS369a	NIS420	NIS424	NIS428
Zone	core	core	core	core	core	core	core	core
SiO_2	45.23	41.67	42.59	45.09	43.65	42.15	42.49	44.97
TiO_2	2.04	3.40	2.89	1.88	2.03	2.60	2.51	2.07
Al_2O_3	8.22	10.92	9.93	9.12	10.67	11.59	11.33	8.34
FeO	16.18	16.61	14.66	14.41	13.51	14.61	14.39	14.70
MnO	0.24	0.18	0.14	0.23	0.16	0.16	0.28	0.30
MgO	12.26	11.11	13.08	13.69	13.86	12.92	13.09	13.33
CaO	11.02	10.59	10.88	10.67	10.74	10.42	11.14	10.98
Na_2O	2.00	2.52	2.23	1.73	1.76	2.60	2.14	1.74
K_2O	0.32	0.40	0.61	0.56	0.47	0.44	0.51	0.41
Cl	0.05	0.07	bdl	0.12	0.17	bdl	0.05	0.12
Sum	97.55	97.47	97.01	97.67	97.01	97.49	97.93	96.97
SiO_2	45.23	41.67	42.59	45.09	43.65	42.15	42.49	44.97
TiO_2	2.04	3.40	2.89	1.88	2.03	2.60	2.51	2.07
Al_2O_3	8.22	10.92	9.93	9.12	10.67	11.59	11.33	8.34
Fe_2O_3	6.60	7.33	8.32	10.26	10.98	10.23	9.18	8.36
FeO	10.24	10.01	7.17	5.18	3.63	5.40	6.13	7.18
MnO	0.24	0.18	0.14	0.23	0.16	0.16	0.28	0.30
MgO	12.26	11.11	13.08	13.69	13.86	12.92	13.09	13.33
CaO	11.02	10.59	10.88	10.67	10.74	10.42	11.14	10.98
Na_2O	2.00	2.52	2.23	1.73	1.76	2.60	2.14	1.74
K_2O	0.32	0.40	0.61	0.56	0.47	0.44	0.51	0.41
Cl	0.05	0.07	0.00	0.12	0.17	0.00	0.05	0.12
H_2O^*	2.03	2.01	2.04	2.05	2.03	2.06	2.05	2.02
Sum	100.24	100.21	99.88	100.74	100.14	100.57	100.90	99.88
O=F,Cl	0.01	0.02	bdl	0.03	0.04	bdl	0.01	0.03
Total	100.23	100.20	99.88	100.72	100.10	100.57	100.89	99.86
Si	6.647	6.176	6.268	6.510	6.316	6.131	6.172	6.581
Al iv	1.353	1.824	1.723	1.490	1.684	1.869	1.828	1.419

(*continued on next page*)

Please cite this article as: F. Mastroianni, E. Braschi and M. Casalini et al., Data on unveiling the occurrence of transient, multi-contaminated mafic magmas inside a rhyolitic reservoir feeding an explosive eruption (Nisyros, Greece), Data in Brief, https://doi.org/10.1016/j.dib.2022.108077

Table 6 (*continued*)

Al vi	0.071	0.084	0.000	0.062	0.135	0.118	0.110	0.020
Cr	0.000	0.000	0.000	0.018	0.000	0.000	0.000	0.006
Fe3+	0.729	0.818	0.921	1.114	1.196	1.120	1.003	0.921
Fe2+	1.259	1.241	0.882	0.626	0.439	0.657	0.745	0.879
Mn	0.030	0.023	0.017	0.029	0.020	0.019	0.034	0.037
Mg	2.686	2.455	2.869	2.947	2.990	2.802	2.833	2.909
Ca	1.736	1.682	1.715	1.650	1.665	1.624	1.734	1.722
Na	0.569	0.725	0.636	0.484	0.495	0.733	0.604	0.494
K	0.061	0.075	0.114	0.103	0.087	0.081	0.094	0.077
Cl	0.012	0.017	0.000	0.028	0.042	0.000	0.013	0.029
OH*	1.988	1.983	2.000	1.972	1.958	2.000	1.987	1.971
Amphibole names	magnesio-hornblende	ferrian-titanian-tschermakite	ferrian-titanian-tschermakitic hornblende	ferri-magnesio-hornblende	ferri-tschermakitic hornblende	ferri-titanian-tschermakite	ferri-titanian-tschermakite	ferrian-magnesio-hornblende
Texture	Type-C	Type-C	Type-C	Type-B	Type-B	Type-B		
Sample	NIS428	NIS428	NIS428	NIS430	NIS430	NIS430		
Zone	core	core	rim	core	rim	core		
SiO_2	46.12	42.69	42.98	45.75	41.93	42.50		
TiO_2	1.43	2.43	2.07	1.69	2.40	2.04		
Al_2O_3	8.29	12.75	11.08	8.64	13.03	12.54		
FeO	13.66	9.25	14.82	15.00	11.99	10.88		
MnO	0.27	0.12	0.18	0.38	0.20	0.18		
MgO	14.24	15.57	12.47	13.39	13.88	14.86		
CaO	10.84	11.54	10.94	10.41	10.82	10.75		
Na_2O	1.54	2.56	2.15	1.74	2.48	1.80		
K_2O	0.30	0.35	0.44	0.36	0.35	0.35		
Cl	0.04	0.01	0.01	0.15	bdl	bdl		
Sum	96.73	97.28	97.14	97.50	97.07	95.89		
SiO_2	46.12	42.69	42.98	45.75	41.93	42.50		
TiO_2	1.43	2.43	2.07	1.69	2.40	2.04		
Al_2O_3	8.29	12.75	11.08	8.64	13.03	12.54		
Fe_2O_3	9.97	6.85	8.26	10.87	9.59	11.99		
FeO	4.69	3.08	7.38	5.22	3.36	0.08		
MnO	0.27	0.12	0.18	0.38	0.20	0.18		
MgO	14.24	15.57	12.47	13.39	13.88	14.86		
CaO	10.84	11.54	10.94	10.41	10.82	10.75		
Na_2O	1.54	2.56	2.15	1.74	2.48	1.80		
K_2O	0.30	0.35	0.44	0.36	0.35	0.35		

(*continued on next page*)

Please cite this article as: F. Mastroianni, E. Braschi and M. Casalini et al., Data on unveiling the occurrence of transient, multi-contaminated mafic magmas inside a rhyolitic reservoir feeding an explosive eruption (Nisyros, Greece), Data in Brief, https://doi.org/10.1016/j.dib.2022.108077

Table 6 (*continued*)

Cl	0.04	0.01	0.01	0.15	bdl	bdl
H_2O^*	2.06	2.09	2.05	2.04	2.08	2.08
Sum	99.83	100.05	100.04	100.70	100.23	99.28
O=F,Cl	0.01	bdl	bdl	0.03	bdl	bdl
Total	99.82	100.05	100.04	100.67	100.23	99.28
Si	6.671	6.126	6.296	6.602	6.052	6.119
Al iv	1.329	1.874	1.704	1.398	1.948	1.881
Al vi	0.083	0.283	0.208	0.071	0.268	0.246
Cr	0.003	0.000	0.004	0.008	0.014	0.011
Fe3+	1.085	0.740	0.911	1.180	1.042	1.299
Fe2+	0.568	0.370	0.904	0.630	0.405	0.010
Mn	0.034	0.015	0.022	0.047	0.024	0.022
Mg	3.071	3.330	2.724	2.880	2.987	3.190
Ca	1.680	1.775	1.717	1.609	1.673	1.658
Na	0.432	0.713	0.610	0.487	0.693	0.503
K	0.055	0.064	0.083	0.067	0.065	0.064
Cl	0.009	0.003	0.002	0.035	0.000	0.000
OH^*	1.991	1.997	1.998	1.965	2.000	2.000
Amphibole names	ferri-magnesio-hornblende	titanian-magnesio-hastingsite	ferrian-tschermakitic hornblende	ferri-magnesio-hornblende	ferri-titanian-tschermakite	ferri-tschermakite

bdl = below detection limit; * calculated on stoichiometric basis. Stoichiometric calculation and nomenclature are from [10].

Please cite this article as: F. Mastroianni, E. Braschi and M. Casalini et al., Data on unveiling the occurrence of transient, multi-contaminated mafic magmas inside a rhyolitic reservoir feeding an explosive eruption (Nisyros, Greece), Data in Brief, https://doi.org/10.1016/j.dib.2022.108077

Table 7
Oxides composition (wt.%) on selected samples from the Upper Pumice deposit (Nisyros, Greece). *Footnotes*: bdl = below detection limit; end-members are calculated following the scheme of [11]: ILM= ilmenite; HEM= hematite; USP=ulvospinel; MT= magnetite.

	ILMENITE-HEMATITE				ULVOSPINEL-MAGNETITE		
Outcrop							
Depositional unit	Fallout	Fallout	Fallout	Lag-breccia	Fallout	Lag-breccia	Lag-breccia
Lithology	Crystal-rich Clast	Crystal-rich Clast	Crystal-rich Clast	Crystal-rich Clast	Pumice	Crystal-rich Clast	Crystal-rich Clast
Texture	Type-B	Type-C	Type-A	Type-A	Porphyritic	Type-B	Type-C
Sample	NIS318	NIS368c	NIS368d	NIS420–23	NIS317	NIS424	NIS428
SiO_2	0.06	0.10	bdl	0.02	0.07	0.06	0.05
TiO_2	43.55	40.90	47.43	42.60	8.36	7.65	6.45
Al_2O_3	0.24	0.25	0.02	0.19	1.56	1.42	1.68
Cr_2O_3	bdl	0.01	bdl	0.05	0.03	bdl	0.09
FeO	52.37	53.07	47.58	52.49	84.56	86.12	86.29
MnO	0.70	0.47	0.47	0.46	0.43	0.35	0.38
MgO	2.16	bdl	0.11	2.17	1.10	0.63	0.45
CaO	bdl	0.06	0.13	bdl	0.06	0.01	0.11
Sum	99.08	94.85	95.73	97.97	96.17	96.23	95.50
SiO_2	0.06	0.10	0.00	0.02	0.07	0.06	0.05
TiO_2	43.55	40.90	47.43	42.60	8.36	7.65	6.45
Al_2O_3	0.24	0.25	0.02	0.19	1.56	1.42	1.68
Cr_2O_3	bdl	0.01	bdl	0.05	0.03	bdl	0.09
Fe_2O_3	19.67	22.45	10.97	20.56	52.40	53.87	55.31
FeO	34.67	32.87	37.70	33.99	37.41	37.64	36.52
MnO	0.70	0.47	0.47	0.46	0.43	0.35	0.38
NiO	bdl	bdl	0.11	bdl	bdl	bdl	bdl
MgO	2.16	1.96	2.35	2.17	1.10	0.63	0.45
CaO	bdl	0.06	0.13	bdl	0.06	0.01	0.11
sum	101.05	99.05	99.18	100.03	101.42	101.63	101.04
Si	0.002	0.003	0.000	0.001	0.00	0.00	0.00
Al	0.007	0.007	0.000	0.005	0.07	0.06	0.07
Cr	0.000	0.000	0.000	0.001	0.00	0.00	0.00

(*continued on next page*)

Please cite this article as: F. Mastroianni, E. Braschi and M. Casalini et al., Data on unveiling the occurrence of transient, multi-contaminated mafic magmas inside a rhyolitic reservoir feeding an explosive eruption (Nisyros, Greece), Data in Brief, https://doi.org/10.1016/j.dib.2022.108077

Table 7 (*continued*)

	ILMENITE-HEMATITE				ULVOSPINEL-MAGNETITE		
Outcrop							
Depositional unit	Fallout	Fallout	Fallout	Lag-breccia	Fallout	Lag-breccia	Lag-breccia
Lithology	Crystal-rich Clast	Crystal-rich Clast	Crystal-rich Clast	Crystal-rich Clast	Pumice	Crystal-rich Clast	Crystal-rich Clast
Fe^{3+}	0.367	0.428	0.207	0.388	1.46	1.51	1.56
Ti	0.812	0.780	0.896	0.802	0.23	0.21	0.18
Mg	0.080	0.074	0.088	0.081	0.06	0.03	0.03
Ni	0.000	0.000	0.002	0.000	0.00	0.00	0.00
Fe^{2+}	0.719	0.697	0.792	0.712	1.16	1.17	1.14
Mn	0.015	0.010	0.010	0.010	0.01	0.01	0.01
Ca	0.000	0.002	0.004	0.000	0.00	0.00	0.00
TiO_2	47.37	46.12	50.01	46.98	12.05	11.00	9.50
FeO	41.93	41.21	44.20	41.68	53.95	54.14	53.82
Fe_2O_3	10.70	12.66	5.79	11.34	34.00	34.86	36.67
ILM'	81.31	78.22	89.60	80.30	21.76	20.63	17.53
HEM'	18.69	21.78	10.40	19.70	74.53	76.44	79.11

bdl = below detection limit; end-members are calculated following the scheme of [10]: ILM= ilmenite; HEM= hematite; USP=ulvospinel; MT= magnetite

2. Experimental Design, Materials and Methods

The field work was carried out with a special care in sampling all of the different juveniles characterising each outcrop of the Upper Pumice deposits. A total of 67 samples (Table 1) was collected during two field campaign in 2006 and 2014.

Pumices were sampled from each location with the aim to investigate the possible variability within the evolved juvenile component for a total of 16 samples (Fig. 1). The CRCs were also sampled in detail, collecting 51 samples, according to their evident textural and physical variability (i.e., density, colour, crystal content) to explore their recurrence and distribution among the different outcrops.

During preparation all specimens were cut in order to remove altered portions, then grinded and powdered in an agate mill.

Major and trace elements were analysed by Actalabs Laboratories (Ontario, Canada) using the Lithogeochemistry-4Lithoresearch analytical package. The procedure consists in a lithium metaborate/tetraborate fusion digestion and analyses are carried out using ICP-OES for major elements and ICP-MS for trace elements (see www.actlabs.com). Accuracy and precision for major elements are estimated as better than 3% for Si, Ti, Fe, Ca, and K, and 7% for Mg, Al, Mn, Na; for trace elements (above 10 ppm) they are better than 10%. REE, Rb, Sr, Y, Zr, Hf, Nb, Th, and U were analysed.

Selected powdered samples were processed in an ultraclean laboratory environment (class 1000) at the Department of Earth Sciences of the University Florence. They were preliminarily treated with 2 mL diluted 1 N HCl in an ultrasonic bath for 15′, twice, then rinsed three times with Milli-Q water to minimise isotopic variation induced by supergene processes that could overprint the magmatic signature (e.g. [12] and references therein). After that they were processed using the standard digestion technique described in [13] consisting in a sequential addition of concentrated HF and HNO_3 (in proportion of 4:1) of suprapure quality, followed by a double addition of concentrated HNO_3, and subsequently by some 10 mL of diluted 6 N HCl and placed on a hot plate at 140°. Cation-exchange AGW and Ln-spec reusable resins were used for Sr, REE and Nd purification respectively, by sequential addition of properly diluted HCl suprapure acid, as described in Avanzinelli et al. [13].

Sr isotope ratios were determined at the Department of Earth Sciences of the University Florence using the Thermal Ionization Thermo-Finnigan Triton-TI mass spectrometer (TIMS), equipped with nine collectors coupled with nine exchangeable amplifiers. For measurements with the thermal ionization mass spectrometer, 100–150 ng of sample were loaded on single Re-filament as nitrate form, with $TaCl_5$ and H_3PO_4 as activator and to keep the signal stable during the analyses. $^{87}Sr/^{86}Sr$ were measured dynamically using the amplifier rotation method and corrected using an exponential mass fractionation law to $^{87}Sr/^{86}Sr$=0.1194. Each ratio is the average of 120 measurements, to reach good precision (2se) of the data. Within run, replicate measurements of international NIST SRM 987 standard (0.710251 ± 0.000011 [13]) gave mean values of $^{87}Sr/^{86}Sr = 0.710252 \pm 0.000011$ (2sd, $n = 5$) well comparable with those reported in literature [14]. All errors reported are 2se (2 standard error of the mean) for single data precisions and 2sd (2 standard deviation) for standards reproducibility (Table 8). The Sr analytical blank, measured during the course of the analytical session, is 60 pg, which is in agreement with blank reproducibility of the lab.

Nd isotope ratios were measured in the Laboratory of Radiogenic Isotopes at the IGG-CNR of Pisa using the new Thermo-Finnigan multicollector inductively coupled plasma mass spectrometer (MC-ICP-MS) Neptune-Plus, equipped with a combined cyclonic and Scott-type quartz spray chamber, Ni-cones, a MicroFlow PFA 100 µl/min self-aspiring nebuliser and a Teledyne Cetac ASX-560 Autosampler. All samples were diluted in ultrapure 2% HNO3 solution after digestion and elemental separation. During Nd analyses, instrumental mass fractionation was corrected using the $^{146}Nd/^{144}Nd$ ratio (0.7219). Mass interference correction was performed using the ratios $^{147}Sm/^{144}Sm$ (4.838710), and $^{147}Sm/^{148}Sm$ (1.327400). The analytical accuracy and reproducibility for the within run internal standard NdFi is 0.511460 ±14 (2sd, $n = 4$), well comparable to

Please cite this article as: F. Mastroianni, E. Braschi and M. Casalini et al., Data on unveiling the occurrence of transient, multi-contaminated mafic magmas inside a rhyolitic reservoir feeding an explosive eruption (Nisyros, Greece), Data in Brief, https://doi.org/10.1016/j.dib.2022.108077

Table 8
Accuracy and reproducibility of Sr-Nd isotopes measurements on international and internal reference standards. *Footnotes:* 2se = 2 standard error of the mean; 2sd = 2 standard deviation.

Method	Multi-dynamic collection mode		
Isotope	Sr ISOTOPE		
Within run standard			
		87Sr/86Sr	**2se**
	SRM987	0.710258	± 0.000005
	SRM987	0.710245	± 0.000006
	SRM987	0.710252	± 0.000005
	SRM987	0.710255	± 0.000006
	SRM987	0.710248	± 0.000005
			2sd
	Average	0.710252	0.000011
Reference	***Thirlwall, 1991***	87Sr/86Sr	2sd
		0.710248	**0.000011**
Instrument	MULTICOLLECTOR INDUCTIVELY COUPLED PLASMA MASS SPECTROMETER - NEPTUNE PLUS		
Method	**Static collection mode**		
Isotope	**Nd ISOTOPE**		
Within run standard			
		143Nd/144Nd	**2se**
	NdFi	0.511464	± 0.000006
	NdFi	0.511451	± 0.000007
	NdFi	0.511466	± 0.000006
	NdFi	0.511460	± 0.000007
			2sd
	Average	0.511460	0.000014
Reference	***Avanzinelli et al., 2005***	143Nd/144Nd	2sd
		0.511467	**0.000008**

2se= 2 standard error of the mean; 2sd= 2 standard deviation

the average value reported in [13] measured by TIMS. Long-term external reproducibility of the laboratory for $^{143}Nd/^{144}Nd$ on international reference material J-Ndi-1 was 0.512098 ± 5 (average of 17 replicates), which match well the reference values of [15], (Table 8).

A number of 10 samples were selected, on the basis of their textural and compositional representativeness, among the different juvenile types (pumices and CRCs) for mineral chemistry investigations on minerals and glasses. Analyses were performed by electron microprobe JEOL Superprobe JXA-8600 at the IGG-CNR of Florence. Working conditions were 15 kV of accelerating voltage and 10 μA of beam current. Beam diameter varied from 2 to 5 μm for mineral phases and 10 for glasses. Peak counting time was 15 sec for major elements, except for Na that is counted for 10 sec to minimize the alkali loss effect, and 40 sec for minor elements. Backgrounds were counted at specific positions for 5 and 20 sec on major and minor elements, respectively.

A set of natural phases (Astimex Albite, Olivine, Diopside, Orthoclase, Plagioclase, Sanidine, Kaersutite, Bustamite, Obsidian and Smithsonian Anorthite *Great Sitikin Islands*, Olivine *San Carlos*, Augite *Kakanui*, Pyrope *Kakanui*, Horneblende *Kakanui*, Ilmenite or Bio-Rad Albite and Orthoclase) and synthetic internal glass standards (ALV-47 and CFA-981) was used as primary and quality control standards. PAP software was used for correction [16]. Precision was within 1% for silica, 2–3% for other major elements and about 5–8% for minor elements.

Scanning Electron Microprobe (SEM) images were achieved at the MEMA laboratory of the University of Florence using 20 kV of acceleration voltage and 2 nA of probe current.

Please cite this article as: F. Mastroianni, E. Braschi and M. Casalini et al., Data on unveiling the occurrence of transient, multi-contaminated mafic magmas inside a rhyolitic reservoir feeding an explosive eruption (Nisyros, Greece), Data in Brief, https://doi.org/10.1016/j.dib.2022.108077

Declaration of Competing Interest

The authors declare that they have no known competing financial interests or personal relationships which have, or could be perceived to have, influenced the work reported in this article.

Data Availability

Data on the juvenile products of the Upper Pumice eruption on Nisyros (Braschi et al., 2022) (Original data) (Earth/Chem).

CRediT Author Statement

F. Mastroianni: Investigation, Writing – review & editing, Visualization; **E. Braschi:** Conceptualization, Investigation, Resources, Data curation, Writing – original draft, Visualization; **M. Casalini:** Methodology, Validation, Writing – review & editing; **S. Agostini:** Methodology, Validation; **S. Di Salvo:** Methodology, Validation; **G. Vougioukalakis:** Investigation, Resources, Writing – review & editing; **L. Francalanci:** Writing – review & editing, Supervision, Project administration, Funding acquisition.

Acknowledgments

The authors sincerely thank all the researchers associated to the Radiogenic Isotopes Laboratory of Florence and Pisa for assistance during analysis and isotope measurements. A special thank to dott.ssa L. Chiarantini for assistance during SEM session. The financial support was provided by Italian MIUR through the PRIN-2017 funding grant 20178LPCPW, issued to LF.

References

[1] E. Braschi, F. Mastroianni, S. Di Salvo, S. Agostini, G.E. Vougioukalakis, L. Francalanci, Unveiling the occurrence of transient, multi-contaminated mafic magmas inside a rhyolitic reservoir feeding an explosive eruption (Nisyros, Greece), Lithos 410–411 (2022) 10657, doi:10.1016/j.lithos.2021.106574.
[2] E.M. Limburg, J.C. Varekamp, Young pumice deposits on Nisyros, Greece, Bull. Volcanol. 54 (1991) 68–77, doi:10.1007/BF00278207.
[3] L. Francalanci, J.C. Varekamp, G. Vougioukalakis, M.J. Defant, F. Innocenti, P. Manetti, Crystal retention, fractionation and crustal assimilation in a convecting magma chamber, Nisyros Volcano, Greece, Bull. Volcanol. 56 (1995) 601–620.
[4] C. Longchamp, C. Bonadonna, O. Bachmann, A. Skopelitis, Characterization of tephra deposits with limited exposure: the example of the two largest explosive eruptions at Nisyros Volcano (Greece), Bull. Volcanol. 73 (2011) 1337–1352, doi:10.1007/s00445-011-0469-9.
[5] J.C. Hardiman, Deep Sea Tephra from Nisyros Island, Eastern Aegean Sea, Greece, 161, Geological Society, London, Special Publications, 1999, pp. 69–88, doi:10.1144/GSL.SP.1999.161.01.06.
[6] M.J. Branney, B.P. Kokelaar, Pyroclastic Density Currents and the Sedimentation of Ignimbrites, Geological Society, 2002, p. 27.
[7] Vougioukalakis, G.E., Blue Volcanoes: Nisyros. Nisyros Regional Council. (1998) 78.
[8] E. Braschi, L. Francalanci, G.E. Vougioukalakis, Inverse differentiation pathway by multiple mafic magma refilling in the last magmatic activity of Nisyros Volcano, Greece, Bull. Volcanol. 74 (2012) 1083–1100, doi:10.1007/s00445-012-0585-1.
[9] S.S. Sun, W.F. McDonough, Chemical and Isotopic Systematics of Oceanic Basalts: Implications for Mantle Composition and Processes, 42, Geological Society, London, Special Publications, 1989, pp. 313–345, doi:10.1144/GSL.SP.1989.042.01.19.
[10] F. Ridolfi, Amp-TB2: an updated model for calcic amphibole thermobarometry, Minerals 11 (2021) 324, doi:10.3390/min11030324.
[11] I.S.E. Carmichael, The mineralogy and petrology of the volcanic rocks from the Leucite Hills, Wyoming, Contrib. Mineral. Petrol. 15 (1967) 24–66, doi:10.1007/BF01167214.
[12] I.G. Nobre Silva, D. Weis, J.S. Scoates, Effects of acid leaching on the Sr-Nd-Hf isotopic compositions of ocean island basalts, Geochem. Geophys. Geosyst. 11 (2010) Q09011, doi:10.1029/2010GC003176.
[13] R. Avanzinelli, E. Boari, S. Conticelli, L. Francalanci, L. Guarnieri, G. Perini, C.M. Petrone, S. Tommasini, M. Ulivi, High precision Sr, Nd, and Pb isotopic analyses using the new generation thermal ionisation mass spectrometer ThermoFinnigan Triton-Ti®, Period. Mineral. 74 (2005) 147–166 3.

Please cite this article as: F. Mastroianni, E. Braschi and M. Casalini et al., Data on unveiling the occurrence of transient, multi-contaminated mafic magmas inside a rhyolitic reservoir feeding an explosive eruption (Nisyros, Greece), Data in Brief, https://doi.org/10.1016/j.dib.2022.108077

[14] M.F. Thirlwall, Long-term reproducibility of multicollector Sr and Nd isotope ratio analysis, Chem. Geol. 94 (1991) 85–104.
[15] N.S. Saji, D. Wielandt, C. Paton, M. Bizzarro, Ultra-high-precision Nd-isotope measurements of geological materials by MC-ICPMS, J. Anal. At. Spectrom. 31 (7) (2016) 1490–1504, doi:10.1039/C6JA00064A.
[16] J.L. Pouchou, F. Pichoir, Quantitative analysis of homogeneous or stratified microvolumes applying the model "PAP", in: K.F.J. Heinrich, D.E. Newbury (Eds.), Electron Probe Quantitation, Springer, Boston, MA, 1991.

Please cite this article as: F. Mastroianni, E. Braschi and M. Casalini et al., Data on unveiling the occurrence of transient, multi-contaminated mafic magmas inside a rhyolitic reservoir feeding an explosive eruption (Nisyros, Greece), Data in Brief, https://doi.org/10.1016/j.dib.2022.108077